

# eScholarship@UMassChan

## Inherent regulatory asymmetry emanating from network architecture in a prevalent autoregulatory motif

Item Type	Accepted Manuscript
Authors	Ali, Zulfikar;Parisutham, Vinuselvi;Choubey, Sandeep;Brewster, Robert C
Citation	<p>&lt;p&gt;Ali MZ, Parisutham V, Choubey S, Brewster RC. Inherent regulatory asymmetry emanating from network architecture in a prevalent autoregulatory motif. Elife. 2020 Aug 18;9:e56517. doi: 10.7554/eLife.56517. Epub ahead of print. PMID: 32808926. &lt;a href="https://doi.org/10.7554/eLife.56517"&gt;Link to article on publisher's site&lt;/a&gt;&lt;/p&gt;</p>
DOI	<a href="https://doi.org/10.7554/eLife.56517">10.7554/eLife.56517</a>
Rights	© 2020, Ali et al. This article is distributed under the terms of the Creative Commons Attribution License permitting unrestricted use and redistribution provided that the original author and source are credited.
Download date	2026-06-16 11:49:32
Item License	<a href="http://creativecommons.org/licenses/by/4.0/">http://creativecommons.org/licenses/by/4.0/</a>
Link to Item	<a href="https://hdl.handle.net/20.500.14038/41537">https://hdl.handle.net/20.500.14038/41537</a>

# Inherent regulatory asymmetry emanating from network architecture in a prevalent autoregulatory motif

Md Zulfikar Ali<sup>1,2†</sup>, Vinuselvi Parisutham<sup>1,2†</sup>, Sandeep Choubey<sup>3</sup>, Robert C. Brewster<sup>1,2\*</sup>

**\*For correspondence:**

[Robert.Brewster@umassmed.edu](mailto:Robert.Brewster@umassmed.edu)  
(FMS)

<sup>†</sup>These authors contributed equally  
to this work

<sup>1</sup>Program in Systems Biology, University of Massachusetts Medical School, 368 Plantation St., Worcester, MA 01605; <sup>2</sup>Department of Microbiology and Physiological Systems, University of Massachusetts Medical School, 368 Plantation St., Worcester, MA 01605.; <sup>3</sup>Max Planck Institute for the Physics of Complex Systems, Nothnitzer strasse 38, 01187 Dresden, Germany

**Abstract** Predicting gene expression from DNA sequence remains a major goal in the field of gene regulation. A challenge to this goal is the connectivity of the network, whose role in altering gene expression remains unclear. Here, we study a common autoregulatory network motif, the negative single-input module, to explore the regulatory properties inherited from the motif. Using stochastic simulations and a synthetic biology approach in *E. coli*, we find that the TF gene and its target genes have inherent asymmetry in regulation, even when their promoters are identical; the TF gene being more repressed than its targets. The magnitude of asymmetry depends on network features such as network size and TF binding affinities. Intriguingly, asymmetry disappears when the growth rate is too fast or too slow and is most significant for typical growth conditions. These results highlight the importance of accounting for network architecture in quantitative models of gene expression.

## Introduction

The genomics revolution has enabled biology with the ability to read, write and assemble DNA at the genome scale with single base pair resolution. These advancements have provided an important tool for the field of gene regulation that aims to predict gene expression from the regulatory code, inscribed in DNA (*Carey et al. (2013)*; *Kosuri et al. (2013)*; *Sharon et al. (2012)*). This approach relies on quantitative measurements of gene expression as the regulatory DNA is systematically designed to induce regulation by various transcription factors (TFs) at specific positions or with differing affinities. However, success in predicting expression levels of natural genes from sequence alone has been relatively modest. One obvious complication is that genes are not isolated but rather exist in dense, interconnected networks. The concept of network motifs, defined as overrepresented patterns of connections between genes and TFs in the network, helps to digest these large networks into smaller subgraphs with specific properties; each of these motifs can be interpreted as performing a particular “information processing” function that is determined by the connectivity and regulatory role of the genes in the motif (*Alon (2006, 2007)*; *Davidson (2006)*; *Mangan and Alon (2003)*; *Tkačik et al. (2008)*). In this study, we dissect a prevalent gene regulation

40 motif, the single-input module (SIM), to demonstrate the influence of network size and connectivity  
41 on the regulation of a network motif.

42 The SIM is a network motif where a single TF regulates the expression of a set of genes, including  
43 itself (Fig. 1A). In *E. coli* this motif is prevalent; the majority of TFs are autoregulated and have  
44 multiple targets (**Santos-Zavaleta et al. (2018)**). Typically, this group of genes have related functions  
45 and the purpose of this motif is to coordinate, in both time and magnitude, expression of these  
46 related genes (**Alon (2006)**). There are mounting examples, from diverse topics that range from  
47 metabolism (Fig. 1B, (**Zaslaver et al. (2004)**)), stress response (Fig. 1C, (**Friedman et al. (2005)**;  
48 **Ronen et al. (2002)**)), development (**Arnone (2002)**; **Gaudet and Mango (2002)**; **Kalir et al. (2001)**),  
49 and cancer (**Lorenzin et al. (2016)**), where temporal ordering of gene expression in the motif  
50 naturally follows the functional order of the genes in the physiological pathway. Mechanistically,  
51 it is thought that this ordering is set through differential affinity for the TF amongst the various  
52 target genes in the motif (**Alon (2006)**), although in some experiments temporal ordering was  
53 not observed implying a dependence on physiology or another experimental detail that is yet  
54 unrecognized (**Gerosa et al. (2013)**; **Schmidt et al. (2016)**). Due to the broad importance of these  
55 motifs, a quantitative understanding of how SIM motifs can be encoded, designed and optimized,  
56 will be instrumental in gaining a deep and fundamental understanding of the spatial and temporal  
57 features of a diverse set of cellular phenomena.

58 To quantitatively explore the input-output relationship of the SIM motif, we use a synthetic  
59 biology approach that boils the motif down to its most basic components: an autoregulated TF  
60 gene, a sample target gene, and competing binding sites. Using *E. coli* as a model organism we build  
61 this motif *in vivo*. We use non-functional “decoy” binding sites to exert competition for the TF and  
62 mimic the demand of the other genes in the motif (which will depend on the size of the network,  
63 Fig. 1D (**Gillespie (1977)**; **Shen-Orr et al. (2002)**). However, the demand for the TF could also stem  
64 from a litany of sources such as random non-functional sites in the genome (**Bakk and Metzler**  
65 **(2004)**; **Kemme et al. (2016)**; **Lee and Maheshri (2012)**; **Mirny (2009)**) or non-DNA based obstruction  
66 or localization effects that transiently interfere with a TFs ability to bind DNA. Because of the design,  
67 our results do not depend on the nature of the TF competition. SIM TFs typically exert the same  
68 regulatory role on all targets of the motif (**Shen-Orr et al. (2002)**). As such, in this work we will focus  
69 on a TF that is a negative regulator of its target genes and itself; this is the most common regulation  
70 strategy in *Escherichia coli* where roughly 60% of TF genes are autoregulated and almost 70% of  
71 those TFs negatively regulate their own expression (inset Fig. 1D, (**Shen-Orr et al. (2002)**)).

72 We use stochastic simulations of kinetic models (**Gillespie (1977, 2007)**; **Kaern et al. (2005)**;  
73 **Shahrezaei and Swain (2008)**), to predict how the overall level of gene expression depends on  
74 parameters characterizing cellular environment such as TF binding affinities and the number of  
75 competing binding sites. To test these predictions *in vivo*, we built a synthetic system with LacI as a  
76 model TF, and individually tune each of these parameters. Past work with LacI has demonstrated the  
77 ability to control with precision the regulatory function, binding affinity and TF copy number through  
78 basic sequence level manipulations (**Brewster et al. (2014)**; **Choi et al. (2008)**; **Garcia and Phillips**  
79 **(2011)**; **Jones et al. (2014)**; **Kuhlman et al. (2007)**; **Oehler et al. (1990)**; **Razo-Mejia et al. (2018)**); Here  
80 we use that detailed knowledge to inform our simulations which then guide our experiments (and  
81 vice versa).

82 Our approach reveals that the presence of competing TF binding sites can have counterintuitive  
83 effects on the mean expression levels of the TF and its target genes due to the opposing relationship  
84 between free TFs and total TFs (total TF is the sum of free TF and TF bound to promoters and  
85 decoy binding sites). Furthermore, we find that the TF and target gene experience quantitatively  
86 different levels of regulation in the same cell, and with the same regulatory sequence. We show  
87 that this regulatory asymmetry is sensitive to features such as the degradation rate, TF binding  
88 affinity and the number of competing binding sites for the TF. The stochastic simulation makes  
89 accurate predictions of the asymmetry and its dependence on the parameters of the model that  
90 we confirm through *in vivo* measurements. Interestingly, regulatory asymmetry is not captured by a

91 simple deterministic model which is based on translating the stochastic reactions to kinetic rates  
 92 through mass action equilibrium kinetics (which have been shown to accurately predict target gene  
 93 expression in other studies (*Brewster et al. (2014)*; *Garcia and Phillips (2011)*; *Garcia et al. (2012)*;  
 94 *Jones et al. (2014)*; *Razo-Mejia et al. (2018)*). In fact, this deterministic model fails to accurately  
 95 predict expression of either gene. A revised deterministic model, which explicitly allows for different  
 96 microenvironments in each “regulatory state”, predicts asymmetry although it still does not recover  
 97 quantitative agreement with stochastic simulations.

## 98 Results

### 99 Matching molecular biology with simulation methodology

100 We use a combination of theory and experimental *in vivo* measurements on engineered *E. coli*  
 101 strains to study the interplay between TF gene, target gene, and additional binding sites of a  
 102 negative autoregulatory SIM network motif. The basic regulatory system is outlined in Fig. 1E. We  
 103 use a stochastic model of the SIM motif to explore how the expression of the TF gene and one  
 104 target gene depends on parameters such as TF binding affinity and number of other binding sites in  
 105 the network (here modeled and controlled through competing, non-regulatory decoy sites (*Burger*  
 106 *et al. (2010)*). In this model, the TF gene and target gene can be independently bound by a free TF  
 107 to shut off gene expression until the TF unbinds. The two genes (TF-encoding and target) compete  
 108 with decoy binding sites which can also bind free TFs. Each free TF can bind any open operator site  
 109 with equal probability (set by the binding rate). The unbinding rate can be set individually for the  
 110 TF gene, target gene and decoy sites and is related to the specific base pair identity of the bound  
 111 operator site (*Kinney et al. (2010)*; *Maerkl and Quake (2007)*; *Stormo (2000)*; *Weirauch et al. (2013)*).  
 112 We employ stochastic simulations to make specific predictions for how the expression level of the TF  
 113 and target genes depend on the various parameters of the model. Furthermore, we translate these  
 114 stochastic processes into a deterministic ODE model using equilibrium mass action kinetics (see  
 115 Appendix 6: Deterministic solution). A thorough discussion on how we chose the kinetic parameters  
 116 of our model is presented in the methods section.

117 In experiments, the corresponding system is constructed with an integrated copy of both the  
 118 TF (LacI-mCherry) and target gene (YFP) with expression of both genes controlled by identical  
 119 promoters with a single LacI binding site centered at +11 relative to their transcription start sites  
 120 (*Brewster et al. (2014)*; *Garcia and Phillips (2011)*). As demonstrated in Fig. 1F, decoy binding sites  
 121 are added by introducing a plasmid with an array of TF binding sites (between 0 to 5 sites per  
 122 plasmid) enabling control of up to roughly 300 binding sites per cell (for average plasmid copy  
 123 number measured by qPCR, see methods and Appendix 3 Figure 1). TF unbinding rate is controlled  
 124 by changing the sequence identity of the operator sites; the binding sequence assessed in this  
 125 study include (in order of increasing affinity) O2, O1 and Oid. The decoy binding site arrays are  
 126 constructed using the Oid operator site. We quantify regulation through measurements of fold-  
 127 change (FC) in expression which is defined as the expression level of a gene in a given condition  
 128 (typically a specific number of decoy binding sites) divided by the expression of that gene when  
 129 it is unregulated. For the target gene we can always measure unregulated expression simply by  
 130 measuring expression in a LacI knockout strain. However, it is challenging to measure unregulated  
 131 expression for the autoregulated gene. For autoregulation this unregulated expression can be  
 132 measured by exchanging the TF binding site with a mutated non-binding version of the site. For O1  
 133 there is a mutated sequence (NoO1v1 *Oehler et al. (1994)*) that we have shown relieves repression  
 134 of the target gene comparable to a strain expressing no TF (see Appendix 4 Figure 1A) which  
 135 allows us to calculate fold-change even for the autorepressed gene. Despite testing many different  
 136 mutated sites and strategies, we could not find a corresponding sequence for O2 and Oid so we  
 137 focus primarily on studying a TF gene regulated by O1 (see Appendix 4: Constitutive values for  
 138 autoregulatory gene, for more discussion).

### 139 **Decoy sites increase expression of the auto-repressed gene and its targets**

140 We first investigate the negatively regulated SIM motif where the TF and target gene have identical  
 141 promoters and TF binding sites (O1) and the number of (identical) competing binding sites are  
 142 varied systematically (schematically shown in Fig. 1E, F). Simulation and experimental data for  
 143 Fold-change of the TF gene as a function of number of decoys is shown in Fig. 2A as red lines  
 144 (simulation) and red points (experiments). We find that increasing the number of decoy sites  
 145 increases the expression of the auto-repressed TF gene monotonically. To interpret why the TF level  
 146 increases, in Fig. 2B we plot the number of “free” TFs in our simulation (defined as TFs not bound to  
 147 an operator site) as a function of decoy site number. The solid line demonstrates that on average,  
 148 despite the increased average number of TFs in the cell, the number of unbound TFs decreases as  
 149 the number of competing binding sites increases (*Nevozhay et al. (2009)*). Therefore, because the  
 150 number of available repressors decreases, the overall level of repression also decreases and thus  
 151 the mean expression of the TF gene rises.

152 Now we consider the effect of competition on the expression of SIM target genes. We measure  
 153 our system with O1 as the regulatory binding site for both TF and target genes. In Fig. 2A, the  
 154 expression of the target gene is shown as blue points (experiments) and blue lines (simulation) for  
 155 the SIM motif with different numbers of decoy TF binding sites (from 0 sites up to 5 per plasmid).  
 156 Just as in the case of the TF gene, we once again see that the expression of the target gene increases  
 157 as more decoy binding sites are added even though the total number of TFs is also increasing (red  
 158 points and line). Qualitatively, we expected this result since the free TF number is expected to  
 159 decrease (Fig. 2B) and, in turn, the expression of any gene targeted by the autoregulated repressing  
 160 TF will increase. While the mechanism is more obvious in this controlled system, it is important to  
 161 note that this is a case where more repressors correlate with more expression of the repressed  
 162 gene. It is easy to see how this relationship could be misinterpreted as activation in more complex  
 163 *in vivo* system if the competition level of the TF is (advertently or otherwise) altered in experiments.

### 164 **Asymmetry in gene regulation between TF and target genes**

165 Quantitative inspection of Fig. 2A reveals an interesting detail: Even when the regulatory region of  
 166 the auto-repressed gene and the target gene are identical, we find that the expression (fold-change  
 167 or FC) is higher for the target gene, raising the question of how two genes with identical promoters  
 168 and regulatory binding sites in the same cell can have different regulation levels. In this data, both  
 169 the TF gene and target gene are regulated by a single repressor binding site (O1) immediately  
 170 downstream of the promoter. This regulatory scheme is often referred to as “simple repression”  
 171 (*Bintu et al. (2005)*; *Garcia and Phillips (2011)*; *Phillips et al. (2013)*). Drawing our intuition from a  
 172 simple deterministic model of regulation based on translating the stochastic reactions to kinetic  
 173 rate equations (Fig. 2C and Appendix 6: Deterministic solution), we find that regardless of the  
 174 network architecture (autoregulation, constitutive TF production, number of competing sites, *etc.*),  
 175 the fold-change of any gene is expected to follow a simple scaling relation,

$$\text{Fold - change} = \frac{1}{1 + R^*},$$

$$R^* = R_{\text{free}} \frac{k_{\text{on}}}{k_{\text{off}} + \gamma}.$$

176 where,  $R_{\text{free}}$  is the number of free (unbound) TFs and  $k_{\text{on}}/(k_{\text{off}} + \gamma)$  represents the affinity of the  
 177 specific TF binding site in the thermodynamic framework (*Rydenfelt et al. (2014)*). This calculation  
 178 is applicable for both the TF and the target gene and would predict a “symmetric” response for  
 179 identical regulatory regions. This model performs well for this same promoter in a related system  
 180 where the TF is induced or constitutively expressed and predicts the fold-change for a wide range of  
 181 perturbations such as promoter strength, TF binding site, induction condition and TF competition  
 182 levels are tuned (data accumulated in Fig. 3A, adapted from (*Phillips et al. (2019)*). However, it has  
 183 been shown that the regulation of an autorepressed gene can diverge from this prediction (*Hahl*

184 *and Kremling (2016); Hornos et al. (2005); Miliás-Argeitis et al. (2015)*). In Fig. 3, we show simulation  
 185 data for the fold-change versus number of scaled-free TFs ( $R^*$ ) for the autoregulatory gene (red line)  
 186 and its target gene (blue line) with O1 (Fig. 3C) or O2 (Fig. 3B) binding sites, where we are changing  
 187 the number of free TFs by tuning the number of competing binding sites. In each plot, we also show  
 188 simulations for the fold-change of a single target gene with a TF undergoing constitutive (constant  
 189 in time) expression where the TF is controlled by either changing the expression level of the TF  
 190 (purple stars) or adding competing binding sites while maintaining a set constitutive expression  
 191 level (purple circles). In both cases, where TFs are made constitutively, the simulation data agrees  
 192 well with the deterministic model predictions. However, for the autoregulatory circuits, we find that  
 193 for strong binding sites (O1) neither the target nor the TF gene follow the deterministic solution  
 194 (black dashed line). In this case, the asymmetry occurs with the TF gene being more repressed and  
 195 the target gene less repressed than expected.

196 Since “free TF concentration” is not readily available in experiments, we demonstrate asymmetry  
 197 in experimental results explicitly in Fig. 3D, where we plot the fold-change of the target gene against  
 198 fold-change of the TF gene. In this figure, the data points are derived from measurements made  
 199 in six different competition levels (from 0 to 5 decoy binding sites per plasmid). Each data point  
 200 represents the average expression level of each gene for a given number of competing binding  
 201 sites. The lines represent results from the stochastic simulations where we systematically vary  
 202 competition levels by introducing decoy binding sites and the fold-change of both the TF and target  
 203 gene are calculated. The simple deterministic model prediction that identical promoters (yellow  
 204 data, Fig. 3D) should experience identical levels of regulation (see Appendix 6 Figure 1C, (*Sanchez*  
 205 *et al. (2011)*)) would cause the data to fall on the black dashed one-to-one line. However, for both  
 206 simulations and experiments of this system the TF gene is clearly more strongly regulated than the  
 207 target gene subject to identical regulatory sequences.

208 To examine the extent of asymmetry in this system, we adjust the target binding site to be of  
 209 higher affinity (Oid, blue lines and data points in Fig. 3D) or weaker (O2, purple lines and data points  
 210 in Fig. 3D). Clearly, this should change the symmetry of the regulation, after all the TF binding sites  
 211 on the promoters are now different and symmetry is no longer to be expected. The experiments  
 212 and simulations once again agree well. However, when Oid regulates the target gene and O1  
 213 regulates the TF gene, the regulation is now roughly symmetric despite the target gene having a  
 214 much stronger binding site; in this case, the size of the inherent regulatory asymmetry effect is on  
 215 par with altering the binding site to a stronger operator resulting in symmetric overall regulation of  
 216 the genes.

### 217 **Mechanism of asymmetric gene regulation**

218 The difference in expression between the TF and its target can be understood by studying the  
 219 TF-operator occupancy for each gene, drawn schematically in Fig. 4A. This cartoon shows the four  
 220 possible promoter occupancy states of the system: (1) both genes unbound by TF, (2) target gene  
 221 bound by TF, TF gene unbound, (3) TF gene bound by TF, target gene unbound, and (4) both genes  
 222 bound by TF. It should be clear that state 1 and state 4 cannot be the cause of asymmetry; both  
 223 genes are either fully on (state 1) or fully off (state 4). As such the asymmetry must originate from  
 224 differences in states 2 and 3. In state 2, the TF gene is “on” while the target gene is fully repressed  
 225 and in state 3 the opposite is true. Since we know that the asymmetry appears as more regulation  
 226 of the TF gene than the target gene, then it must be the case that the system spends less time in  
 227 state 2 than in state 3. There are two paths to exit either of these states: unbinding of the TF from  
 228 the bound operator or binding of the TF to the free operator. Since unbinding rate of a TF is identical  
 229 for both promoters in our model, the asymmetry must originate from differences in binding of free  
 230 TF in state 2 and in state 3; specifically state 2 must have an (on average) higher concentration of  
 231 TF than state 3. This makes sense since the system is still making TF in state 2, while production  
 232 of TF is shut off in state 3. Fig. 4B validates this interpretation as we can see that state 2 has on  
 233 average more free TFs than state 3, and as a result, the system spends less time in state 2 than

234 in state 3 in our simulations. As such, the asymmetry comes from the fact that the two genes,  
 235 despite being in the same cell and experiencing the same average intracellular TF concentrations,  
 236 are exposed to systematically different concentrations of TF when the TF and target gene are in their  
 237 respective “active” states. To quantify regulatory asymmetry, we define asymmetry as the difference  
 238 in fold-change of the target and the fold-change of the TF gene (asymmetry =  $FC_{\text{target}} - FC_{\text{TF}}$ ). Using  
 239 the chemical master equation (CME) approach, we find that the asymmetry is exactly equal to the  
 240 difference in time spent in state 3 and state 2, for any condition or parameter choice (Fig. 4C and  
 241 Appendix 9 Eqn. A9-9: CME for minimal model). Furthermore, the asymmetry can be written as the  
 242 difference of TF concentration in state 2 and state 3 and is given by

$$\text{Asymmetry} = \frac{k_{\text{on}}}{k_{\text{off}} + \gamma} (n_2 - n_3),$$

243 where,  $n_2$  and  $n_3$  are the TF concentrations in state 2 and state 3, respectively. In Fig. 4D we show  
 244 that the asymmetry obtained using the difference in TF concentration precisely match with the  
 245 asymmetry calculated from the fold-change expression. However, it is important to note, that this  
 246 is not a complete analytic solution for asymmetry because  $n_2$  and  $n_3$  are unsolved functions of the  
 247 model parameters.

248 The asymmetry in the expression of TF and target genes stems from systematically differential  
 249 TF concentration in the states when the TF gene is occupied (and target gene is expressing) and  
 250 when the target gene is occupied (and the TF gene is expressing). The general approach of ODEs  
 251 outlined above (Fig. 2C) does not account for this differential TF concentration and hence shows no  
 252 asymmetry. Armed with the knowledge that individual states have this systematic TF difference,  
 253 we can rewrite the basic deterministic model where we instead keep track individually of each  
 254 state and the specific TF concentration of that state using the same equilibrium mass action kinetic  
 255 approach (details in Appendix 10: Modified ODEs for the minimal model). Like the stochastic CMEs  
 256 the modified ODEs predict that the asymmetry arises from the difference in the TF concentrations  
 257 in different states and solely depends on the difference in time spent in state 3 (only target gene  
 258 occupied) and state 2 (only TF gene occupied). Although we find the modified deterministic model  
 259 can predict asymmetry, it still does not quantitatively agree with the results of stochastic modeling  
 260 due to the deterministic model not accounting for variability in TF number in each state (see  
 261 Appendix 10: Modified ODEs for the minimal model). As a result, in the following sections, we will  
 262 compare our experiments to stochastic simulations based on the full CME formalism.

### 263 **Dependence of regulatory asymmetry on TF degradation and binding affinity**

264 According to the above proposed mechanism, the regulatory asymmetry stems from differences  
 265 in the cellular TF concentration when the TF is bound to the target versus when it is bound to  
 266 the autoregulatory gene, as such we expect that binding affinity will play a central role in setting  
 267 asymmetry levels. This is also evident from Fig. 3B, C where we find that the deviation of the  
 268 expression of both TF and target gene is more prominent for a strong binding site (Oid or O1)  
 269 compared to a weaker binding site (O2). Furthermore, there are many parameters associated  
 270 with the production and decay of TF and target mRNA and protein which could also influence the  
 271 asymmetry. To reveal which (if any) of these parameters is important to asymmetry, we calculate  
 272 the maximum asymmetry (the maximum value of asymmetry found as competing site number is  
 273 controlled, Appendix 7 Figure 1A) using simulation as these production and degradation parameters  
 274 are tuned. First, we find that tuning the rates of target gene production and decay has no effect on  
 275 asymmetry (Appendix 7 Figure 1B and Appendix 11 Figure 1B). On the other hand, for TF production  
 276 and decay each parameter has some effect on asymmetry. However, we find that the biggest driver  
 277 of asymmetry in this set of parameters is the protein degradation rate (Appendix 7 Figure 1B).  
 278 As such, we focus on two crucial parameters that control the asymmetry: TF binding affinity and  
 279 TF degradation rate. In Fig. 4E we show a heat map of the maximum asymmetry as a function  
 280 of the rate of protein degradation and binding affinity of the TF. We see from this figure that

281 strong binding produces enhanced asymmetry, but the degradation rate displays an interesting  
 282 intermediate maximum in asymmetry – degradation that is too fast, or too slow will not show  
 283 asymmetry, but a maximum asymmetry is expected for TF lifetimes between 10 and 100 minutes.  
 284 Crucially, this maximum coincides with typical doubling time of *E. coli* (which sets the TF half-life  
 285 (Marr (1991); Neidhardt and Curtiss (1996)) and thus regulatory asymmetry in this motif is most  
 286 relevant in common physiological conditions.

287 The non-monotonic behavior of asymmetry with degradation rate of TF can be explained by the  
 288 TF-promoter occupancy (alternatively, residence time) of the TF and the target gene. Analytically,  
 289 the asymmetry is given by the difference of occupancy of state 2 and state 3 (Appendix 9 Eqn. A9-7:  
 290 CME for minimal model). For slow degradation, the number of TFs in a cell is high, favoring the  
 291 transition to state 4 very quickly, thereby reducing the residence times of both state 2 and 3. On the  
 292 other extreme, when degradation is fast, the TF number is too low for the cell to be in the state 2 or  
 293 3; the cell spends most of the time in state 1. In both the cases, the difference of residence times  
 294 between state 2 and state 3 is low and hence the asymmetry is small. In the intermediate regime of  
 295 degradation, the number of TFs is optimum to maximize the difference between residence times in  
 296 state 2 and 3, which leads to maximum asymmetry.

297 To experimentally test the theory predictions for the role of TF degradation in setting regulatory  
 298 asymmetry, we introduced several *ssrA* degradation tags to the *Lacl* in our experiments (McGinness  
 299 *et al.* (2006)). The data, shown in Fig. 4F includes degradation by a “weak” or “slow” tag (DAS with  
 300 a rate of 0.00063 per minute per enzyme (McGinness *et al.* (2007)), blue points), a slightly faster  
 301 tag (DAS+4 with a rate of 0.0011 per minute per enzyme (McGinness *et al.* (2007)), green points)  
 302 and a very fast tag (LAA tag with a rate of 0.21 per minute per enzyme (McGinness *et al.* (2007)),  
 303 red points) . In addition, the data without a tag is shown as yellow points. Here we see that the  
 304 slowest tag (blue points) introduces strong asymmetry. However, for the next fastest tag (green  
 305 points) we see a significant decrease in asymmetry and the level of regulatory asymmetry is similar  
 306 to what is seen in the absence of tags (yellow points). Finally, the fastest tag (red points) shows  
 307 no asymmetry at all. It is worth pointing out that the qualitative order of degradation rates in  
 308 these experiments can be inferred from how far the data “reaches”, faster degradation will lead  
 309 to higher overall fold-changes for a given competition level. Importantly, controlling the protein  
 310 degradation rate through this synthetic tool agrees with our model predictions, although the actual  
 311 *in vivo* protein degradation rates are difficult to estimate from tag sequence alone, the asymmetry  
 312 follows the expected trends based on the known (and observed) effectiveness of each tag (see  
 313 schematic inset Fig. 4F).

314 In the absence of targeted degradation, the degradation rate of most protein in *E. coli*, is naturally  
 315 set by the growth rate. According to the model predictions in Fig. 4E, the asymmetry should be  
 316 highest for fast growing cells (roughly 20-minute division rate for our growth conditions which is  
 317 well below the degradation rate for peak asymmetry ~ 10 minutes, Fig. 4F) and decrease (or vanish)  
 318 for very slow growing cells. To test this, we take the system with O1 regulatory binding sites on  
 319 both the target and the TF promoter (yellow data in Fig. 3D grown in M9 + glucose, 55-minute  
 320 doubling time) and grow in a range of doubling times between 22 minutes (rich defined media) up  
 321 to 215 minutes (M9 + acetate) (see Appendix 2 Figure 1A). Importantly, when we change the growth  
 322 rate, other rates such as the transcription and translation rates will also be impacted (Bremer and  
 323 Dennis (2008); Klumpp *et al.* (2009)), while these parameters will change the quantitative values of  
 324 the asymmetry curve, the qualitative ordering and features of the asymmetry are not expected to  
 325 be impacted (see Appendix 11 Figure 1C). The data for these growth conditions is shown in Fig. 5A.  
 326 As predicted, faster growing cells show more regulatory asymmetry and slower growing cells show  
 327 little-to-no regulatory asymmetry. We also test the role of growth rate in asymmetric regulation  
 328 when O2 (a lower affinity site) and Oid (a higher affinity site) are used as the regulatory binding sites  
 329 instead of O1. This data is shown in Fig. 5B (O2) and 5C (Oid). As discussed above, we could not find  
 330 a suitable mutant for O2 and Oid that both relieved regulation from *Lacl* and completely restored  
 331 the expression of target gene (see Appendix 4: Constitutive values for autoregulatory gene.). This

332 means we cannot explicitly measure the 1-1 correlation between the two axes in our data when  
 333 using O2 or Oid for the TF gene. To this end, we find this correspondence by fitting the glucose data  
 334 to our simulation of the same system and use that value to normalize all other growth rates for that  
 335 operator. Despite this complication, it is clear that O2 regulation is symmetric at all studied growth  
 336 rates while Oid regulation is asymmetric for all growth rates with faster growth rates appearing  
 337 more asymmetric.

338 Importantly, the regulatory asymmetry is not due to a small population of outliers, bimodality  
 339 or any other “rare” phenotype. In Fig. 5D, we show a histogram of single cell asymmetry values  
 340 (defined as  $\text{asymmetry} = FC_{\text{Target}} - FC_{\text{TF}}$ ) for each condition. As can be seen, expression in each  
 341 media condition are roughly symmetric for most cells at the lowest competition levels (top panel).  
 342 However, as competition levels are increased, the fast-growing conditions shift to higher asymmetry  
 343 levels; strikingly at the highest growth rate almost every single cell is expressing target at a higher  
 344 level than TF (bottom panel).

## 345 Discussion

346 The single-input module (SIM) is a prevalent regulation strategy in both bacteria (*Ma et al. (2004);*  
 347 *Shen-Orr et al. (2002)*) and higher organisms (*Lee et al. (2002); Segal et al. (2003); Yu et al. (2003)*).  
 348 While the role of TF autoregulation (positive and negative) has been extensively studied (*Acar*  
 349 *et al. (2008); Assaf et al. (2011); Becskei and Serrano (2000); Ochab-Marcinek et al. (2017); Rodrigo*  
 350 *et al. (2016); Rosenfeld et al. (2002); Savageau (1975); Semsey et al. (2009)*), the focus here is on  
 351 the combined influence of an autoregulated TF and its target genes and how the shared need  
 352 for that TF influences the quantitative features of its regulatory behaviors. We find that there  
 353 is a fundamental asymmetry in gene regulation that can occur in the SIM regulatory motif. This  
 354 asymmetry is not related to distinctions in the biological processes or an unexpected difference  
 355 in our *in vivo* experiment, but rather an inherent asymmetry originating from the way the motif  
 356 itself is wired. Although two identical promoters are in the same cell with the same average protein  
 357 concentrations, they experience distinct regulatory environments. This is particularly relevant  
 358 for the SIM motif because the primary function of the motif, organizing and coordinating gene  
 359 expression patterns, operates on the premise of differential affinities amongst target genes; here  
 360 we have shown that the TF gene has an inherent “affinity advantage” due to being exposed to  
 361 systematically higher TF concentrations than its target genes. This implies that the TF gene will  
 362 respond “earlier” than expected based on the raw affinity of its binding site and may necessitate  
 363 weaker sites on autoregulating TF genes in order to achieve similar timing in expression compared  
 364 to its targets. This may also shed light on the discrepancies in Arg pathway timing between different  
 365 experiments which have used plasmid reporters (essentially changing network size) or different  
 366 physiological growth conditions; the asymmetry is critically sensitive to both of these features.  
 367 Although, here we are using *E. coli* as a model organism where it is easy to build and manipulate  
 368 these regulatory motifs, we expect this phenomenon to apply broadly to other regulatory systems.

369 Regulatory asymmetry is intrinsic to the negative SIM motif even in the absence of decoys, but  
 370 it can be greatly exacerbated by competing TF binding sites. Due to the promiscuous nature of  
 371 TF binding, this highlights the importance of considering not just the “closed” system of a TF and  
 372 a given target but also the impact of other binding sites (or inactivating interactions) for the TF  
 373 in predicting regulation as well as the regulatory motif at play in the system. In our system, the  
 374 magnitude of the asymmetry is enough to compensate for swapping the wild-type proximal O1 LacI  
 375 binding site on the target gene with the “ideal” operator Oid.

376 The cause of this asymmetry is a systematic difference in the TF concentration when the TF gene  
 377 is active compared to when the target gene is active. As such, asymmetry is magnified by anything  
 378 that enhances this concentration difference. Here we have identified TF binding affinity and TF  
 379 degradation rate (controlled both directly and through modulating growth rate) as primary drivers  
 380 of asymmetry in this motif. Although the relationship between growth rate and expression levels  
 381 is well established (*Bremer and Dennis (2008); Klumpp and Hwa (2008); Klumpp et al. (2009); Scott*

382 *et al. (2010); Volkmer and Heinemann (2011)*), effects such as this add a layer of complexity to this  
383 relationship.

384 In studies of quantitative gene regulation, the typical goal is to predict the output of a gene based  
385 on the regulatory composition of that gene's promoter and the number and identity of regulatory  
386 proteins. This work clearly presents a challenge for the drive to "read" and predict regulation  
387 levels from the promoter DNA alone, in this case the regulatory motif is responsible for altering  
388 the observed regulation and must be considered as well. It has previously been demonstrated  
389 that features of a transcript can impact its regulation by effects such as targeted degradation,  
390 stabilization or posttranslational modification and regulation (*Schikora-Tamarit et al. (2018)*), it is  
391 important to point out that regulatory asymmetry in this motif is a distinct phenomenon that does  
392 not operate through an enzymatic processes but rather is a fundamental feature of the network.

393 Finally, here we demonstrate regulatory asymmetry using a specific (but common) regulatory  
394 motif. The more general problem of quantifying the role of asymmetry in other network motifs  
395 may be an important step in expanding the predictive power of models based on single genes. The  
396 broader point that specific genes can be exposed to systematically different levels of regulatory TFs  
397 even in the absence of specific cellular mechanisms such as cytoplasmic compartmentalization,  
398 protein localization or DNA accessibility is likely more generally relevant. Understanding and  
399 quantifying these mechanisms can be an important piece towards improving our ability to predict  
400 and design gene regulatory circuits.

#### 401 **Acknowledgments**

402 We wish to thank Rob Phillips, Griffin Chure, Manuel Razo-Mejia, Amir Mitchell, Job Dekker, Marian  
403 Walhout, and Michael Lee for helpful discussions. We thank Dr. Jeffrey Bailey for providing us with  
404 qubit for DNA quantification. We thank Kenan Murphy for his valuable suggestions on protein  
405 degradation tags. We declare no conflict of interest. Funding: Research reported in this publication  
406 was supported by NIGMS of the National Institutes of Health under award R35GM128797. Author  
407 contributions: MA did the computational analysis; VP performed all the experiments; SC provided  
408 the necessary supervision for the computational setup; RB conceptualized the experiments and  
409 drafted the manuscript. All data and codes are backed up in UMASS server. We have uploaded the  
410 full source code to repeat the simulations in the following link: [GitHub link](#).

411 **Materials and Methods**

Key Resources Table				
Reagent type (species) resources	Designation	Source or reference	Identifiers	Additional information
gene ( <i>E. coli</i> )	<i>ybcN</i> <>25XX+ 11- <i>lacI-mcherry</i>	GeneBank	MT726947	TF gene; XX can be O1, O2 or Oid operator
gene ( <i>E. coli</i> )	<i>galk</i> <>3*5XX+ 11- <i>yfp</i>	GeneBank	MT726948	Target gene; XX can be O1, O2 or Oid operator
strain, strain background ( <i>E. coli</i> )	<i>E. coli</i> MG1655	Lab stock	CGSC#6300	Wild type
strain, strain background ( <i>E. coli</i> )	HG105	<i>Garcia and Phillips (2011)</i>		<i>E. coli</i> MG1655 with <i>lac</i> operon deleted
strain, strain background ( <i>E. coli</i> )	HG105 $\Delta$ <i>sspB</i>	This study		<i>E. coli</i> HG105 with <i>sspB</i> gene deleted
Other	M9 minimal media	BD Diagnostics	DF0485-17	commercial media
Other	Rich defined media	Teknova	#M2105	commercial media
software, algorithm	Matlab code	Schnitzcells <i>Rosenfeld et al. (2005)</i>		
Other	C code for simulations	<a href="#">GitHub link</a> This study		

412 **Bacterial Strains**

413 All strains used in this study are constructed from the parent strain *E. coli* HG105 which is MG1655  
414 with the *lac* operon deleted (MG1655 $\Delta$ *lacIZYA*). Auto-regulated TF (*lacI-mCherry*) is expressed  
415 from the *ybcN* locus and the TF-repressed target (*yfp*) is expressed from the *galk* locus with identical  
416 promoter sequence for both the TF and the target. Decoys are introduced on the pZE plasmid. In  
417 order to tune the degradation rate of the TF, three different *ssrA* tags were added to the C-terminus  
418 of the *LacI-mCherry* fusion protein. The tags used in this study are wildtype LAA tag (AANDENYALAA),  
419 DAS tag (AANDENYADAS) and DAS+4 tag (AANDENYSENADAS)(*McGinness et al. (2006)*). For protein  
420 degradation tag experiments with *LacI-mCherry* fusion protein, HG105 with  $\Delta$ *sspB* knockout is used  
421 as a parent strain to substantially moderate the protein degradation rate. It is also noteworthy that  
422 deletion of *sspB* gene did not affect the growth rate in any of the strains tested. Primers used in this  
423 study are listed in Table 1.

424 **Microscopy**

425 Bacterial cultures are grown overnight in 1 mL of LB in a 37°C incubator shaking at 250 rpm. Unless  
426 otherwise stated cultures grown overnight are diluted  $2.5 \times 10^3$  fold to an initial OD of 0.002 into  
427 1 mL of fresh M9 minimal media supplemented with 0.5% of one of the three different carbon

428 sources (Glucose, Glycerol or Acetate) or in Rich Defined Media (RDM, Teknova #M2105), allowed to  
 429 grow at 37°C until they reach an OD600 of 0.2 to 0.4 (0.1 for acetate) and harvested for microscopy.  
 430 Cells are diluted 1:3 in 1X PBS (in order to obtain isolated cells in microscope images) and 1  $\mu$ L is  
 431 spotted on a 2% low melting agarose pad (Invitrogen #16520050) made with 1X PBS. Cells grown in  
 432 RDM are cross-linked with paraformaldehyde before imaging to prevent shrinkage and osmotic  
 433 shock to the cells. An automated fluorescent microscope (Nikon TI-E) with a heating chamber set at  
 434 37°C is used to record multiple fields per sample (between 8-12 unique fields of view) resulting in  
 435 roughly 500 to 1000 individual cells per sample.

### 436 **qPCR measurements for average plasmid copy number**

437 We performed qPCR measurements in order to quantify the average copy number of the pZE  
 438 plasmid. Cells are grown as described for microscopic analysis and diluted 1:200 in Qiagen P1 lysis  
 439 buffer and allowed to sit on ice. Meanwhile, cells are plated at 10<sup>-5</sup> dilutions on fresh LB plates in  
 440 order to determine the colony forming units per mL (CFU/mL). 25  $\mu$ L of the lysate is diluted with 25  
 441  $\mu$ L of 1X PBS and allowed to sit for 5 minutes. The cells are then diluted 1:100 into 1X cut smart  
 442 buffer from NEB. 20  $\mu$ L of the mixture is incubated with 0.5  $\mu$ L of HindIII restriction enzyme for 30  
 443 minutes at 37°C followed by heat inactivation at 80°C for 20 minutes. The mixture is further diluted  
 444 1:10 and 4.2  $\mu$ L is used as a template in a 20  $\mu$ L qPCR reaction mixture. The pZE-1XOid plasmid is  
 445 purified using the Qiagen Plasmid Mini Prep kit and quantified using the Qubit dsDNA assay kit. A  
 446 standard curve is then prepared by diluting pZE-1XOid plasmid from 10<sup>8</sup> copies down to 10 copies.  
 447 The average copy number of the decoy plasmid per cell is computed by comparing the cT of the  
 448 sample to the standard curve and dividing by the number of cells in the sample.

### 449 **Simulation methodology**

450 To model the experiments and study the effect of decoy sites on the expression of a target gene  
 451 regulated by a negatively autoregulated TF gene, we develop a simple model of the experimental  
 452 system. In our model the auto-regulatory gene produces a protein ( $X$ ) which forms a TF dimer  
 453 ( $R$ ). We explicitly modeled TF as a dimer to incorporate the fact that LacI acts as a dimer in our  
 454 experimental system (the LacI-mCherry construct lacks the tetramerization domain (*Kipper et al.*  
 455 *(2018)*). Dimerization and de-dimerization steps occur at the rate  $k_p$  and  $k_m$ , respectively. The  
 456 TF binds to its own promoter ( $P_{TF}$ ), to the promoter of the target gene ( $P_{target}$ ), and to the decoy  
 457 sites ( $N$ ) with a constant rate  $k_{on}$  per free TF per unit time. The off rate of the bound TF ( $k_{off}$ , the  
 458 unbinding rate) depends on the sequence identity and can be different for different promoters.  
 459 A bound TF unbinds from the promoters of the TF and target, and from the decoy sites at a rate  
 460  $k_{off,TF}$ ,  $k_{off,target}$  and  $k_{off,decoy}$  per unit time, respectively. A TF-free promoter produces an mRNA at  
 461 the rate  $\beta$  which is then translated into a protein at a rate  $\alpha$ . The mRNA and the proteins are  
 462 degraded at the rate  $\gamma_m$  and  $\gamma$ , respectively. We assume that all proteins (free protein, TF bound to  
 463 promoter and TF bound to decoy sites) degrades with the same rate. Typically, the proteins in *E.*  
 464 *coli* are very stable with protein half-life greater than the cell cycle and the dominant contribution  
 465 to degradation comes from the dilution due to cell division. The degradation rate is thus given by  
 466  $\gamma = \ln(2)/\tau_1 + \ln(2)/\tau_2$ , where  $\tau_1$  and  $\tau_2$  are protein half-life and cell division time, respectively. The  
 467 set of reactions describing the model above are listed in Appendix Figure 2A.

468 We implement the simulations for stochastic reaction systems using Gillespie's algorithm (*Gille-*  
 469 *spie (1977)*) in C programming. Each simulation is run for sufficiently long time ( $\sim 10^6$  s) to reach  
 470 a steady state. Typically, for the rates used in this paper the steady state is achieved in 10<sup>5</sup> s or  
 471 less (see Appendix 6 Figure 1 for a sample time trace). Data for steady state distributions (TF and  
 472 target protein) are then recorded by sampling over time with a time interval ( $T_s$ ) long enough for  
 473 the slowest reaction to occur 20 times on average ( $T_s = 20$  over rate for slowest reaction). Mean  
 474 protein numbers in steady state for fold-change are calculated using at least 10<sup>5</sup> data points for  
 475 each single run.

## 476 Kinetic parameter estimation

477 To compare the results from experiments with our simulations we are required to find values for  
 478 the kinetic on and off rate of LacI for different operator sites (Oid, O1 and O2), the transcription  
 479 and translation rates, mRNA degradation rate, and the growth rates in different media. We directly  
 480 measure growth rate for different media in our experiment (see Appendix 2). The on and off rates  
 481 are related to the binding energy ( $\Delta\epsilon$ ) through,

$$\frac{k_{\text{on}}}{k_{\text{off}} + \gamma} = \frac{\exp(-\Delta\epsilon)}{N_{\text{ns}}}, \quad (1)$$

482 where  $N_{\text{ns}} \sim 5 \times 10^6$  bps is the number of non-specific binding sites in the genome (which we  
 483 take as the total number of bases) (Phillips *et al.* (2013)),  $k_{\text{on}}$  is the binding rate per free TF per  
 484 unit time,  $k_{\text{off}}$  is the unbinding rate per unit time and  $\gamma$  is the decay rate of the TF. Experimental  
 485 measurements of  $\Delta\epsilon$  have been reported in many repeated experiments (Brewster *et al.* (2014);  
 486 Garcia and Phillips (2011); Razo-Mejia *et al.* (2018)) and thus we constrain our choice of  $k_{\text{on}}$  and  
 487  $k_{\text{off}}$  such that we obtain affinities consistent with these measurements. Taking one data set (O1  
 488 regulated TF and O1 regulated target grown in glucose), we use maximum likelihood analysis to  
 489 obtain the rates by varying  $k_{\text{on}}$  in a range 0.0015-0.003  $s^{-1}$  (which sets the corresponding value of  
 490  $k_{\text{off}}$  to give  $\Delta\epsilon_{\text{O1}} = 15.3k_{\text{B}}T$ ) (Elf *et al.* (2007); Bremer and Dennis (2008)),  $\gamma_{\text{m}}^{-1}$  in a range of 30-90 s (Yu  
 491 *et al.* (2006); Bremer and Dennis (2008)),  $\beta$  in a range of 0.1-0.3  $s^{-1}$  (Kennell and Riezman (1977)),  
 492 and choosing  $\alpha$  (Cai *et al.* (2006)) such that the constitutive number for the TF protein is in the range  
 493 of 1000-2600; this parameter largely sets the “range” of our fold-change vs fold-change curves and  
 494 this range of  $\alpha$  reproduces the experimental range we see in those curves for this data set.

495 We then use this same on rate to derive the relevant off rates for O2 and Oid using their  
 496 binding energies ( $\Delta\epsilon_{\text{O2}} = 13.9k_{\text{B}}T$ ,  $\Delta\epsilon_{\text{Oid}} = 16.3k_{\text{B}}T$ ) and Equation 1. Interestingly, the binding affinity  
 497 we measure for Oid is 0.7  $k_{\text{B}}T$  weaker than has been previously reported but is consistent with  
 498 measurements of Oid binding affinity in our lab. Using this method, we find the  $k_{\text{on}}$  to be 0.0015 per  
 499 TF per second, which yields  $k_{\text{off}}$  to be, O1=0.0015  $s^{-1}$ , O2 = 0.0167  $s^{-1}$  and Oid=0.0004  $s^{-1}$ , consistent  
 500 with previous findings (Elf *et al.* (2007); Hammar *et al.* (2014); Jones *et al.* (2014); Razo-Mejia *et al.*  
 501 (2018)). All other rates are listed in Table 2. Importantly, this process is not meant to precisely  
 502 determine the exact quantitative parameters of LacI binding, and it is not a formal fit, but rather  
 503 an estimate that provides us with realistic prediction of regulation from our simulations using  
 504 molecular parameters that are consistent with available direct kinetic measurements (Chen *et al.*  
 505 (2015); Elf *et al.* (2007); Sanchez *et al.* (2011); Yu *et al.* (2006)).

## 506 Data Analysis

507 Data analysis is performed using a modified version of the Matlab code Schnitzcells (Rosenfeld  
 508 *et al.* (2005)). We use this code to segment the phase images of each sample to identify single  
 509 cells. Mean pixel intensities of YFP and mCherry signals are extracted from the segmented phase  
 510 mask for each individual cell using regionprops, an inbuilt function in matlab. The background  
 511 fluorescence is calculated by averaging the mean intensity of the inverse phase mask upon eroding  
 512 the regions around the segmented cell masks. The background fluorescence value of a particular  
 513 frame was subtracted from the mean pixel intensity of cells in the same frame (see Appendix 1).  
 514 Finally, the autofluorescence value were calculated using the same procedure for cells that do not  
 515 express either YFP or mCherry and the average autofluorescence value of these cells is subtracted  
 516 from each measured YFP or mCherry value. Resulting mean pixel intensity of mCherry signal was  
 517 corrected for the crosstalk from YFP signal. Crosstalk between different channels can be measured  
 518 by determining the difference between the autofluorescence of a strain without a given fluorophore  
 519 in the presence of the other fluorophore (highly expressed). We find that under our microscope  
 520 0.25% ( $\gamma_{\text{cross}} = 0.0025$ ) of YFP signals can be seen in the mCherry channel whereas mCherry channel  
 521 has no crosstalk in the YFP channel. Hence, we correct for this crosstalk by subtracting the mean  
 522 pixel intensity of YFP signal times the  $\gamma_{\text{cross}}$  from the mean pixel intensity of mCherry signal. The

523 per-pixel fluorescence values of mCherry and YFP of each cell is then multiplied by the area of the  
 524 cell to account for the total fluorescence. Fold-change in expression of the mCherry and YFP is  
 525 calculated by dividing the corresponding values of the constitutive strains (discussed in Appendix  
 526 4). At least 500 individual cells were analyzed per sample and binned according to the mCherry  
 527 values. Any bin with less than 50 data points is excluded. Unless otherwise stated, each data point  
 528 represents the bootstrapped mean of all data points in a given bin and the error bar represents the  
 529 standard deviation of the bootstrapped mean.

## 530 References

- 531 **Acar M**, Mettetal JT, van Oudenaarden A. Stochastic Switching as a Survival Strategy in Fluctuating Environments.  
 532 *Nature Genetics*. 2008; 40(4):471–475. <https://doi.org/10.1038/ng.110>, doi: 10.1038/ng.110.
- 533 **Alon U**. An Introduction to Systems Biology: Design Principles of Biological Circuits. Taylor & Francis; 2006.  
 534 <https://books.google.com/books?id=tcxClxzCO4C>.
- 535 **Alon U**. Network Motifs: Theory and Experimental Approaches. *Nature Reviews Genetics*. 2007; 8(6):450–461.  
 536 <https://doi.org/10.1038/nrg2102>, doi: 10.1038/nrg2102.
- 537 **Arnone MI**. Bringing Order to Organogenesis. *Nature Genetics*. 2002; 30(4):348–350. <https://doi.org/10.1038/ng0402-348>, doi: 10.1038/ng0402-348.
- 539 **Assaf M**, Roberts E, Luthey-Schulten Z. Determining the Stability of Genetic Switches: Explicitly Accounting for  
 540 mRNA Noise. *Physical Review Letters*. 2011; 106(24):248102. <https://link.aps.org/doi/10.1103/PhysRevLett.106.248102>, doi: 10.1103/PhysRevLett.106.248102.
- 542 **Bakk A**, Metzler R. Nonspecific Binding of the OR Repressors CI and Cro of Bacteriophage . *Journal of Theoretical*  
 543 *Biology*. 2004; 231(4):525–533. <http://www.sciencedirect.com/science/article/pii/S0022519304003285>, doi:  
 544 <https://doi.org/10.1016/j.jtbi.2004.07.007>.
- 545 **Becskei A**, Serrano L. Engineering Stability in Gene Networks by Autoregulation. *Nature*. 2000; 405(6786):590–  
 546 593. <https://doi.org/10.1038/35014651>, doi: 10.1038/35014651.
- 547 **Bintu L**, Buchler NE, Garcia HG, Gerland U, Hwa T, Kondev J, Phillips R. Transcriptional Regulation by the Numbers:  
 548 Models. *Current Opinion in Genetics & Development*. 2005; 15(2):116–124. <http://www.sciencedirect.com/science/article/pii/S0959437X05000304>, doi: <https://doi.org/10.1016/j.gde.2005.02.007>.
- 550 **Bremer H**, Dennis P. Modulation of Chemical Composition and Other Parameters of the Cell at Different  
 551 Exponential Growth Rates. *EcoSal Plus*. 2008; <https://www.asmscience.org/content/journal/ecosalplus/10.1128/ecosal.5.2.3>, doi: doi:10.1128/ecosal.5.2.3.
- 553 **Brewster R**, Weinert F, Garcia H, Song D, Rydenfelt M, Phillips R. The Transcription Factor Titration Effect Dictates  
 554 Level of Gene Expression. *Cell*. 2014; 156(6):1312–1323. <http://www.sciencedirect.com/science/article/pii/S0092867414002219>, doi: <https://doi.org/10.1016/j.cell.2014.02.022>.
- 556 **Burger A**, Walczak AM, Wolynes PG. Abduction and Asylum in the Lives of Transcription Factors. *Proceedings of*  
 557 *the National Academy of Sciences*. 2010; 107(9):4016–4021. [https://www.pnas.org/content/pnas/107/9/4016](https://www.pnas.org/content/pnas/107/9/4016.full.pdf).  
 558 [full.pdf](https://doi.org/10.1073/pnas.0915138107), doi: 10.1073/pnas.0915138107.
- 559 **Cai L**, Friedman N, Xie XS. Stochastic protein expression in individual cells at the single molecule level. *Nature*.  
 560 2006; 440(7082):358–62. <https://doi.org/10.1038/nature04599>, doi: 10.1038/nature04599.
- 561 **Carey LB**, van Dijk D, Sloot PMA, Kaandorp JA, Segal E. Promoter Sequence Determines the Relationship  
 562 between Expression Level and Noise. *PLOS Biology*. 2013; 11(4):e1001528. <https://doi.org/10.1371/journal.pbio.1001528>, doi: 10.1371/journal.pbio.1001528.
- 564 **Chen H**, Shiroguchi K, Ge H, Xie XS. Genome-wide Study of mRNA Degradation and Transcript Elongation in  
 565 *Escherichia coli*. *Molecular Systems Biology*. 2015; 11(1):781. <https://www.emboPress.org/doi/abs/10.15252/msb.20145794>, doi: 10.15252/msb.20145794.
- 567 **Choi PJ**, Cai L, Frieda K, Xie XS. A Stochastic Single-Molecule Event Triggers Phenotype Switching of a Bacterial  
 568 Cell. *Science*. 2008; 322(5900):442–446. <https://science.sciencemag.org/content/sci/322/5900/442.full.pdf>,  
 569 doi: 10.1126/science.1161427.

- 570 **Cooper S**, Helmstetter CE. Chromosome replication and the division cycle of *Escherichia coli* Br. *Journal of*  
571 *Molecular Biology*. 1968; 31(3):519–540. <http://www.sciencedirect.com/science/article/pii/0022283668904257>,  
572 [doi: https://doi.org/10.1016/0022-2836\(68\)90425-7](https://doi.org/10.1016/0022-2836(68)90425-7).
- 573 **Davidson EH**. *The Regulatory Genome: Gene Regulatory Networks in Development and Evolution*. Elsevier  
574 Science; 2006. <https://books.google.com/books?id=xMCfngEACAAJ>.
- 575 **Elf J**, Li GW, Xie XS. Probing Transcription Factor Dynamics at the Single-Molecule Level in a Living Cell. *Sci-*  
576 *ence*. 2007; 316(5828):1191–1194. <https://science.sciencemag.org/content/sci/316/5828/1191.full.pdf>, [doi: 10.1126/science.1141967](https://doi.org/10.1126/science.1141967).
- 578 **Friedman N**, Vardi S, Ronen M, Alon U, Stavans J. Precise Temporal Modulation in the Response of the SOS DNA  
579 Repair Network in Individual Bacteria. *PLOS Biology*. 2005; 3(7):e238. <https://doi.org/10.1371/journal.pbio.0030238>, [doi: 10.1371/journal.pbio.0030238](https://doi.org/10.1371/journal.pbio.0030238).
- 581 **Garcia HG**, Phillips R. Quantitative Dissection of the Simple Repression Input–Output Function. *Proceedings of*  
582 *the National Academy of Sciences*. 2011; 108(29):12173–12178. [https://www.pnas.org/content/pnas/108/29/](https://www.pnas.org/content/pnas/108/29/12173.full.pdf)  
583 [12173.full.pdf](https://www.pnas.org/content/pnas/108/29/12173.full.pdf), [doi: 10.1073/pnas.1015616108](https://doi.org/10.1073/pnas.1015616108).
- 584 **Garcia H**, Sanchez A, Boedicker J, Osborne M, Gelles J, Kondev J, Phillips R. Operator Sequence  
585 Alters Gene Expression Independently of Transcription Factor Occupancy in Bacteria. *Cell Re-*  
586 *ports*. 2012; 2(1):150–161. <http://www.sciencedirect.com/science/article/pii/S2211124712001647>, [doi: https://doi.org/10.1016/j.celrep.2012.06.004](https://doi.org/10.1016/j.celrep.2012.06.004).
- 588 **Gaudet J**, Mango SE. Regulation of Organogenesis by the *Caenorhabditis elegans* FoxA Protein PHA-4. *Science*.  
589 2002; 295(5556):821–825. <https://science.sciencemag.org/content/sci/295/5556/821.full.pdf>, [doi: 10.1126/sci-](https://doi.org/10.1126/science.1065175)  
590 [ence.1065175](https://doi.org/10.1126/science.1065175).
- 591 **Gerosa L**, Kochanowski K, Heinemann M, Sauer U. Dissecting specific and global transcriptional regulation of  
592 bacterial gene expression. *Molecular Systems Biology*. 2013; 9(1):658. [https://www.embopress.org/doi/abs/](https://www.embopress.org/doi/abs/10.1038/msb.2013.14)  
593 [10.1038/msb.2013.14](https://www.embopress.org/doi/abs/10.1038/msb.2013.14), [doi: 10.1038/msb.2013.14](https://doi.org/10.1038/msb.2013.14).
- 594 **Gillespie DT**. Exact Stochastic Simulation of Coupled Chemical Reactions. *The Journal of Physical Chemistry*.  
595 1977; 81(25):2340–2361. <https://doi.org/10.1021/j100540a008>, [doi: 10.1021/j100540a008](https://doi.org/10.1021/j100540a008).
- 596 **Gillespie DT**. Stochastic Simulation of Chemical Kinetics. *Annual Review of Physical Chemistry*. 2007; 58(1):35–  
597 55. <https://www.annualreviews.org/doi/abs/10.1146/annurev.physchem.58.032806.104637>, [doi: 10.1146/an-](https://doi.org/10.1146/annurev.physchem.58.032806.104637)  
598 [nurev.physchem.58.032806.104637](https://doi.org/10.1146/annurev.physchem.58.032806.104637).
- 599 **Hahl SK**, Kremling A. A Comparison of Deterministic and Stochastic Modeling Approaches for Biochemical  
600 Reaction Systems: On Fixed Points, Means, and Modes. *Frontiers in Genetics*. 2016; 7(157). [https://www.](https://www.frontiersin.org/article/10.3389/fgene.2016.00157)  
601 [frontiersin.org/article/10.3389/fgene.2016.00157](https://www.frontiersin.org/article/10.3389/fgene.2016.00157), [doi: 10.3389/fgene.2016.00157](https://doi.org/10.3389/fgene.2016.00157).
- 602 **Hammar P**, Walldén M, Fange D, Persson F, Baltekin O, Ullman G, Leroy P, Elf J. Direct Measure-  
603 ment of Transcription Factor Dissociation Excludes a Simple Operator Occupancy Model for Gene  
604 Regulation. *Nature Genetics*. 2014; 46:405. <https://doi.org/10.1038/ng.2905>, [doi: 10.1038/ng.2905](https://doi.org/10.1038/ng.2905)  
605 <https://www.nature.com/articles/ng.2905#supplementary-information>.
- 606 **Hornos JEM**, Schultz D, Innocentini GCP, Wang J, Walczak AM, Onuchic JN, Wolynes PG. Self-regulating gene: An  
607 exact solution. *Physical Review E*. 2005; 72(5):051907. <https://link.aps.org/doi/10.1103/PhysRevE.72.051907>,  
608 [doi: 10.1103/PhysRevE.72.051907](https://doi.org/10.1103/PhysRevE.72.051907).
- 609 **Jones DL**, Brewster RC, Phillips R. Promoter Architecture Dictates Cell-to-Cell Variability in Gene Expression.  
610 *Science*. 2014; 346(6216):1533–1536. <https://science.sciencemag.org/content/sci/346/6216/1533.full.pdf>, [doi: 10.1126/science.1255301](https://doi.org/10.1126/science.1255301).
- 612 **Jun S**, Si F, Pugatch R, Scott M. Fundamental principles in bacterial physiology—history, recent progress, and  
613 the future with focus on cell size control: a review. *Reports on Progress in Physics*. 2018; 81(5):056601.  
614 <http://dx.doi.org/10.1088/1361-6633/aaa628>, [doi: 10.1088/1361-6633/aaa628](https://doi.org/10.1088/1361-6633/aaa628).
- 615 **Kaern M**, Elston TC, Blake WJ, Collins JJ. Stochasticity in Gene Expression: From Theories to Phenotypes. *Nature*  
616 *Reviews Genetics*. 2005; 6(6):451–464. <https://doi.org/10.1038/nrg1615>, [doi: 10.1038/nrg1615](https://doi.org/10.1038/nrg1615).
- 617 **Kalir S**, McClure J, Pabbaraju K, Southward C, Ronen M, Leibler S, Surette MG, Alon U. Ordering Genes in a  
618 *Flagella* Pathway by Analysis of Expression Kinetics from Living Bacteria. *Science*. 2001; 292(5524):2080–2083.  
619 <https://science.sciencemag.org/content/sci/292/5524/2080.full.pdf>, [doi: 10.1126/science.1058758](https://doi.org/10.1126/science.1058758).

- 620 **Kemme CA**, Nguyen D, Chattopadhyay A, Iwahara J. Regulation of Transcription Factors via Natural Decoys in  
621 Genomic DNA. *Transcription*. 2016; 7(4):115–120. <https://www.ncbi.nlm.nih.gov/pubmed/27384377>  
622 <https://www.ncbi.nlm.nih.gov/pmc/articles/PMC4984682/>, doi: 10.1080/21541264.2016.1188873.
- 623 **Kennell D**, Riezman H. Transcription and translation initiation frequencies of the *Escherichia coli* lac  
624 operon. *Journal of Molecular Biology*. 1977; 114(1):1–21. [http://www.sciencedirect.com/science/article/  
625 pii/0022283677902790](http://www.sciencedirect.com/science/article/pii/0022283677902790), doi: [https://doi.org/10.1016/0022-2836\(77\)90279-0](https://doi.org/10.1016/0022-2836(77)90279-0).
- 626 **Kinney JB**, Murugan A, Callan CG, Cox EC. Using Deep Sequencing to Characterize the Biophysical Mechanism of  
627 a Transcriptional Regulatory Sequence. *Proceedings of the National Academy of Sciences*. 2010; 107(20):9158–  
628 9163. <https://www.pnas.org/content/pnas/107/20/9158.full.pdf>, doi: 10.1073/pnas.1004290107.
- 629 **Kipper K**, Eremina N, Marklund E, Tubasum S, Mao G, Lehmann LC, Elf J, Deindl S. Structure-guided approach  
630 to site-specific fluorophore labeling of the lac repressor LacI. *PLOS ONE*. 2018; 13(6):e0198416. <https://doi.org/10.1371/journal.pone.0198416>, doi: 10.1371/journal.pone.0198416.
- 632 **Klumpp S**, Hwa T. Growth-Rate-Dependent Partitioning of RNA Polymerases in Bacteria. *Proceedings of the*  
633 *National Academy of Sciences*. 2008; 105(51):20245–20250. [https://www.pnas.org/content/pnas/105/51/  
634 20245.full.pdf](https://www.pnas.org/content/pnas/105/51/20245.full.pdf), doi: 10.1073/pnas.0804953105.
- 635 **Klumpp S**, Zhang Z, Hwa T. Growth Rate-Dependent Global Effects on Gene Expression in Bacteria. *Cell*.  
636 2009; 139(7):1366–1375. <https://www.ncbi.nlm.nih.gov/pubmed/20064380>  
637 <https://www.ncbi.nlm.nih.gov/pmc/articles/PMC2818994/>, doi: 10.1016/j.cell.2009.12.001.
- 638 **Kosuri S**, Goodman DB, Cambray G, Mutalik VK, Gao Y, Arkin AP, Endy D, Church GM. Composability of regulatory  
639 sequences controlling transcription and translation in *Escherichia coli*. *Proceedings of the National*  
640 *Academy of Sciences*. 2013; 110(34):14024–14029. <https://www.pnas.org/content/pnas/110/34/14024.full.pdf>,  
641 doi: 10.1073/pnas.1301301110.
- 642 **Kuhlman T**, Zhang Z, Saier MH, Hwa T. Combinatorial Transcriptional Control of the Lactose Operon of  
643 *Escherichia coli*. *Proceedings of the National Academy of Sciences*. 2007; 104(14):6043–6048. [https://www.  
644 pnas.org/content/pnas/104/14/6043.full.pdf](https://www.pnas.org/content/pnas/104/14/6043.full.pdf), doi: 10.1073/pnas.0606717104.
- 645 **Kuhlman TE**, Cox EC. Gene location and DNA density determine transcription factor distributions in *Escherichia*  
646 *coli*. *Molecular Systems Biology*. 2012; 8(1):610. <https://www.embopress.org/doi/abs/10.1038/msb.2012.42>,  
647 doi: 10.1038/msb.2012.42.
- 648 **Lee TH**, Maheshri N. A Regulatory Role for Repeated Decoy Transcription Factor Binding Sites in Target Gene  
649 Expression. *Molecular Systems Biology*. 2012; 8(1):576. [https://www.embopress.org/doi/abs/10.1038/msb.  
650 2012.7](https://www.embopress.org/doi/abs/10.1038/msb.2012.7), doi: 10.1038/msb.2012.7.
- 651 **Lee TI**, Rinaldi NJ, Robert F, Odom DT, Bar-Joseph Z, Gerber GK, Hannett NM, Harbison CT, Thompson CM, Simon  
652 I, Zeitlinger J, Jennings EG, Murray HL, Gordon DB, Ren B, Wyrick JJ, Tagne JB, Volkert TL, Fraenkel E, Gifford DK,  
653 et al. Transcriptional Regulatory Networks in *Saccharomyces cerevisiae*. *Science*. 2002; 298(5594):799–804.  
654 <https://science.sciencemag.org/content/sci/298/5594/799.full.pdf>, doi: 10.1126/science.1075090.
- 655 **Lorenzin F**, Benary U, Baluapuri A, Walz S, Jung LA, von Eyss B, Kisker C, Wolf J, Eilers M, Wolf E. Different  
656 Promoter Affinities Account for Specificity in MYC-Dependent Gene Regulation. *eLife*. 2016; 5:e15161.  
657 <https://doi.org/10.7554/eLife.15161>, doi: 10.7554/eLife.15161.
- 658 **Ma HW**, Kumar B, Ditges U, Gunzer F, Buer J, Zeng AP. An Extended Transcriptional Regulatory Network of  
659 *Escherichia coli* and Analysis of its Hierarchical Structure and Network Motifs. *Nucleic Acids Research*. 2004;  
660 32(22):6643–6649. <https://doi.org/10.1093/nar/gkh1009>, doi: 10.1093/nar/gkh1009.
- 661 **Maerkl SJ**, Quake SR. A Systems Approach to Measuring the Binding Energy Landscapes of Transcription Factors.  
662 *Science*. 2007; 315(5809):233–237. <https://science.sciencemag.org/content/sci/315/5809/233.full.pdf>, doi:  
663 10.1126/science.1131007.
- 664 **Mangan S**, Alon U. Structure and Function of the Feed-Forward Loop Network Motif. *Proceedings of the National*  
665 *Academy of Sciences*. 2003; 100(21):11980–11985. <https://www.pnas.org/content/pnas/100/21/11980.full.pdf>,  
666 doi: 10.1073/pnas.2133841100.
- 667 **Marr AG**. Growth Rate of *Escherichia coli*. *Microbiological reviews*. 1991; 55(2):316–333. [https://www.ncbi.nlm.  
668 nih.gov/pubmed/1886524](https://www.ncbi.nlm.nih.gov/pubmed/1886524)<https://www.ncbi.nlm.nih.gov/pmc/articles/PMC372817/>.

- 669 **McGinness KE**, Baker TA, Sauer RT. Engineering Controllable Protein Degradation. *Molecular*  
670 *Cell*. 2006; 22(5):701–707. <http://www.sciencedirect.com/science/article/pii/S1097276506003261>, doi:  
671 <https://doi.org/10.1016/j.molcel.2006.04.027>.
- 672 **McGinness KE**, Bolon DN, Kaganovich M, Baker TA, Sauer RT. Altered Tethering of the SspB Adaptor to the ClpXP  
673 Protease Causes Changes in Substrate Delivery. *Journal of Biological Chemistry*. 2007; 282(15):11465–11473.  
674 <http://www.jbc.org/content/282/15/11465.abstract>, doi: 10.1074/jbc.M610671200.
- 675 **Milias-Argeitis A**, Engblom S, Bauer P, Khammash M. Stochastic focusing coupled with negative feed-  
676 back enables robust regulation in biochemical reaction networks. *Journal of The Royal Society In-*  
677 *terface*. 2015; 12(113):20150831. <https://royalsocietypublishing.org/doi/abs/10.1098/rsif.2015.0831>, doi:  
678 [doi:10.1098/rsif.2015.0831](https://doi.org/10.1098/rsif.2015.0831).
- 679 **Mirny L**. Nucleosome-Mediated Cooperativity Between Transcription Factors. *Nature Precedings*. 2009; <https://doi.org/10.1038/npre.2009.2796.1>, doi: 10.1038/npre.2009.2796.1.
- 681 **Neidhardt FC**, Curtiss R. *Escherichia coli* and *Salmonella*: Cellular and Molecular Biology. ASM Press; 1996.  
682 <https://books.google.com/books?id=haqnQAACAAJ>.
- 683 **Nevozhay D**, Adams RM, Murphy KF, Josić K, Balázsi G. Negative autoregulation linearizes the  
684 dose–response and suppresses the heterogeneity of gene expression. *Proceedings of the National*  
685 *Academy of Sciences*. 2009; 106(13):5123–5128. <https://www.pnas.org/content/pnas/106/13/5123.full.pdf>,  
686 doi: 10.1073/pnas.0809901106.
- 687 **Ochab-Marcinek A**, Jędrak J, Tabaka M. Hill Kinetics as a Noise Filter: the Role of Transcription Fac-  
688 tor Autoregulation in Gene Cascades. *Physical Chemistry Chemical Physics*. 2017; 19(33):22580–22591.  
689 <http://dx.doi.org/10.1039/C7CP00743D>, doi: 10.1039/C7CP00743D.
- 690 **Oehler S**, Amouyal M, Kolkhof P, von Wilcken-Bergmann B, Müller-Hill B. Quality and Position of the Three  
691 lac Operators of *E. coli* Define Efficiency of Repression. *The EMBO journal*. 1994; 13(14):3348–3355. <https://www.ncbi.nlm.nih.gov/pubmed/8045263><https://www.ncbi.nlm.nih.gov/pmc/articles/PMC395232/>.
- 692 **Oehler S**, Eismann ER, Krämer H, Müller-Hill B. The Three Operators of the lac Operon Cooperate in Repression.  
693 *The EMBO Journal*. 1990; 9(4):973–979. [https://www.embopress.org/doi/abs/10.1002/j.1460-2075.1990.](https://www.embopress.org/doi/abs/10.1002/j.1460-2075.1990.tb08199.x)  
694 [tb08199.x](https://www.embopress.org/doi/abs/10.1002/j.1460-2075.1990.tb08199.x), doi: 10.1002/j.1460-2075.1990.tb08199.x.
- 695 **Phillips R**, Kondev J, Theriot J, Garcia H. *Physical Biology of the Cell*. Garland Science; 2013. <https://books.google.com/books?id=iTBvQgAACAAJ>.
- 696 **Phillips R**, Belliveau NM, Chure G, Garcia HG, Razo-Mejia M, Scholes C. Figure 1 Theory Meets Figure 2  
697 Experiments in the Study of Gene Expression. *Annual Review of Biophysics*. 2019; 48(1):121–163. <https://www.annualreviews.org/doi/abs/10.1146/annurev-biophys-052118-115525>, doi: 10.1146/annurev-biophys-052118-115525.
- 698 **Razo-Mejia M**, Barnes SL, Belliveau NM, Chure G, Einav T, Lewis M, Phillips R. Tuning Transcriptional Regulation  
699 through Signaling: A Predictive Theory of Allosteric Induction. *Cell Systems*. 2018; 6(4):456–469.e10. <https://doi.org/10.1016/j.cels.2018.02.004>, doi: 10.1016/j.cels.2018.02.004.
- 700 **Rodrigo G**, Bajic D, Elola I, Poyatos JF. Antagonistic Autoregulation Speeds up a Homogeneous Response in  
701 *Escherichia coli*. *Scientific Reports*. 2016; 6:36196. <https://doi.org/10.1038/srep36196>, doi: 10.1038/srep36196  
<https://www.nature.com/articles/srep36196#supplementary-information>.
- 702 **Ronen M**, Rosenberg R, Shraiman BI, Alon U. Assigning Numbers to the Arrows: Parameterizing a  
703 Gene Regulation Network by Using Accurate Expression Kinetics. *Proceedings of the National Academy*  
704 *of Sciences*. 2002; 99(16):10555–10560. <https://www.pnas.org/content/pnas/99/16/10555.full.pdf>, doi:  
705 [10.1073/pnas.152046799](https://doi.org/10.1073/pnas.152046799).
- 706 **Rosenfeld N**, Elowitz MB, Alon U. Negative Autoregulation Speeds the Response Times of Transcription  
707 Networks. *Journal of Molecular Biology*. 2002; 323(5):785–793. <http://www.sciencedirect.com/science/article/pii/S0022283602009944>, doi: [https://doi.org/10.1016/S0022-2836\(02\)00994-4](https://doi.org/10.1016/S0022-2836(02)00994-4).
- 708 **Rosenfeld N**, Young JW, Alon U, Swain PS, Elowitz MB. Gene Regulation at the Single-Cell Level. *Science*. 2005;  
709 307(5717):1962–1965. <https://science.sciencemag.org/content/sci/307/5717/1962.full.pdf>, doi: 10.1126/sci-  
710 [ence.1106914](https://doi.org/10.1126/science.1106914).
- 711 **Rosenfeld N**, Young JW, Alon U, Swain PS, Elowitz MB. Gene Regulation at the Single-Cell Level. *Science*. 2005;  
712 307(5717):1962–1965. <https://science.sciencemag.org/content/sci/307/5717/1962.full.pdf>, doi: 10.1126/sci-  
713 [ence.1106914](https://doi.org/10.1126/science.1106914).

- 718 **Rydenfelt M**, Cox RS, Garcia H, Phillips R. Statistical mechanical model of coupled transcription from multiple  
719 promoters due to transcription factor titration. *Physical Review E*. 2014; 89(1):012702. [https://link.aps.org/](https://link.aps.org/doi/10.1103/PhysRevE.89.012702)  
720 [doi/10.1103/PhysRevE.89.012702](https://doi.org/10.1103/PhysRevE.89.012702), doi: 10.1103/PhysRevE.89.012702.
- 721 **Sanchez A**, Garcia HG, Jones D, Phillips R, Kondev J. Effect of Promoter Architecture on the Cell-to-Cell Variability  
722 in Gene Expression. *PLOS Computational Biology*. 2011; 7(3):e1001100. [https://doi.org/10.1371/journal.pcbi.](https://doi.org/10.1371/journal.pcbi.1001100)  
723 [1001100](https://doi.org/10.1371/journal.pcbi.1001100), doi: 10.1371/journal.pcbi.1001100.
- 724 **Santos-Zavaleta A**, Salgado H, Gama-Castro S, Sánchez-Pérez M, Gómez-Romero L, Ledezma-Tejeida D, García-  
725 Sotelo JS, Alquicira-Hernández K, Muñoz-Rascado LJ, Peña-Loredo P, Ishida-Gutiérrez C, Velázquez-Ramírez DA,  
726 Del Moral-Chávez V, Bonavides-Martínez C, Méndez-Cruz CF, Galagan J, Collado-Vides J. RegulonDB v 10.5:  
727 Tackling Challenges to Unify Classic and High Throughput Knowledge of Gene Regulation in *E. coli* K-12. *Nucleic*  
728 *Acids Research*. 2018; 47(D1):D212–D220. <https://doi.org/10.1093/nar/gky1077>, doi: 10.1093/nar/gky1077.
- 729 **Savageau MA**. Significance of Autogenously Regulated and Constitutive Synthesis of Regulatory Proteins in  
730 Repressible Biosynthetic Systems. *Nature*. 1975; 258(5532):208–214. <https://doi.org/10.1038/258208a0>, doi:  
731 10.1038/258208a0.
- 732 **Shikora-Tamarit MA**, Lopez-Grado I, Salinas G, Gonzalez-Navasa C, Calderón I, Marcos-Fa X, Sas  
733 M, Carey LB. Promoter Activity Buffering Reduces the Fitness Cost of Misregulation. *Cell Re-*  
734 *ports*. 2018; 24(3):755–765. <http://www.sciencedirect.com/science/article/pii/S2211124718309860>, doi:  
735 <https://doi.org/10.1016/j.celrep.2018.06.059>.
- 736 **Schmidt A**, Kochanowski K, Vedelaar S, Ahrné E, Volkmer B, Callipo L, Knoops K, Bauer M, Aebersold R, Heine-  
737 mann M. The quantitative and condition-dependent *Escherichia coli* proteome. *Nature Biotechnology*. 2016;  
738 34(1):104–110. <https://doi.org/10.1038/nbt.3418>, doi: 10.1038/nbt.3418.
- 739 **Scott M**, Gunderson CW, Mateescu EM, Zhang Z, Hwa T. Interdependence of Cell Growth and Gene Expression:  
740 Origins and Consequences. *Science*. 2010; 330(6007):1099–1102. [https://science.sciencemag.org/content/sci/](https://science.sciencemag.org/content/sci/330/6007/1099.full.pdf)  
741 [330/6007/1099.full.pdf](https://science.sciencemag.org/content/sci/330/6007/1099.full.pdf), doi: 10.1126/science.1192588.
- 742 **Segal E**, Shapira M, Regev A, Pe'er D, Botstein D, Koller D, Friedman N. Module Networks: Identifying Regula-  
743 tory Modules and their Condition-Specific Regulators from Gene Expression Data. *Nature Genetics*. 2003;  
744 34(2):166–176. <https://doi.org/10.1038/ng1165>, doi: 10.1038/ng1165.
- 745 **Semsey S**, Krishna S, Erdossy J, Horváth P, Orosz L, Sneppen K, Adhya S. Dominant Negative Autoregulation Limits  
746 Steady-State Repression Levels in Gene Networks. *Journal of bacteriology*. 2009; 191(14):4487–4491. <https://www.ncbi.nlm.nih.gov/pubmed/19429616><https://www.ncbi.nlm.nih.gov/pmc/articles/PMC2704710/>, doi:  
747 [10.1128/JB.00056-09](https://www.ncbi.nlm.nih.gov/pmc/articles/PMC2704710/).  
748
- 749 **Shahrezaei V**, Swain PS. Analytical Distributions for Stochastic Gene Expression. *Proceedings of the National*  
750 *Academy of Sciences*. 2008; 105(45):17256–17261. <https://www.pnas.org/content/pnas/105/45/17256.full.pdf>,  
751 doi: 10.1073/pnas.0803850105.
- 752 **Sharon E**, Kalma Y, Sharp A, Raveh-Sadka T, Levo M, Zeevi D, Keren L, Yakhini Z, Weinberger A, Segal E. Inferring  
753 gene regulatory logic from high-throughput measurements of thousands of systematically designed promot-  
754 ers. *Nature Biotechnology*. 2012; 30(6):521–530. <https://doi.org/10.1038/nbt.2205>, doi: 10.1038/nbt.2205.
- 755 **Shen-Orr SS**, Milo R, Mangan S, Alon U. Network Motifs in the Transcriptional Regulation Network of *Escherichia*  
756 *coli*. *Nature Genetics*. 2002; 31(1):64–68. <https://doi.org/10.1038/ng881>, doi: 10.1038/ng881.
- 757 **Stamatakis M**, Zygourakis K. Deterministic and stochastic population-level simulations of an artificial lac  
758 operon genetic network. *BMC Bioinformatics*. 2011; 12(1):301. <https://doi.org/10.1186/1471-2105-12-301>,  
759 doi: 10.1186/1471-2105-12-301.
- 760 **Stormo GD**. DNA Binding Sites: Representation and Discovery. *Bioinformatics*. 2000; 16(1):16–23. <https://doi.org/10.1093/bioinformatics/16.1.16>, doi:  
761 [10.1093/bioinformatics/16.1.16](https://doi.org/10.1093/bioinformatics/16.1.16).
- 762 **Tkačik G**, Callan CG, Bialek W. Information Flow and Optimization in Transcriptional Regulation. *Proceedings of*  
763 *the National Academy of Sciences*. 2008; 105(34):12265–12270. [https://www.pnas.org/content/pnas/105/34/](https://www.pnas.org/content/pnas/105/34/12265.full.pdf)  
764 [12265.full.pdf](https://www.pnas.org/content/pnas/105/34/12265.full.pdf), doi: 10.1073/pnas.0806077105.
- 765 **Volkmer B**, Heinemann M. Condition-Dependent Cell Volume and Concentration of *Escherichia coli* to Facilitate  
766 Data Conversion for Systems Biology Modeling. *PLOS ONE*. 2011; 6(7):e23126. [https://doi.org/10.1371/journal.](https://doi.org/10.1371/journal.pone.0023126)  
767 [pone.0023126](https://doi.org/10.1371/journal.pone.0023126), doi: 10.1371/journal.pone.0023126.

- 768 **Weinert FM**, Brewster RC, Rydenfelt M, Phillips R, Kegel WK. Scaling of Gene Expression with Transcription-  
769 Factor Fugacity. *Physical Review Letters*. 2014; 113(25):258101. [https://link.aps.org/doi/10.1103/PhysRevLett.](https://link.aps.org/doi/10.1103/PhysRevLett.113.258101)  
770 [113.258101](https://link.aps.org/doi/10.1103/PhysRevLett.113.258101), doi: [10.1103/PhysRevLett.113.258101](https://doi.org/10.1103/PhysRevLett.113.258101).
- 771 **Weirauch MT**, Cote A, Norel R, Annala M, Zhao Y, Riley TR, Saez-Rodriguez J, Cokelaer T, Vedenko A,  
772 Talukder S, Consortium D, Agius P, Arvey A, Bucher P, Callan Jr CG, Chang CW, Chen CY, Chen YS,  
773 Chu YW, Grau J, et al. Evaluation of Methods for Modeling Transcription Factor Sequence Speci-  
774 ficity. *Nature Biotechnology*. 2013; 31:126. <https://doi.org/10.1038/nbt.2486>, doi: [10.1038/nbt.2486](https://doi.org/10.1038/nbt.2486)  
775 <https://www.nature.com/articles/nbt.2486#supplementary-information>.
- 776 **Yu H**, Luscombe NM, Qian J, Gerstein M. Genomic Analysis of Gene Expression Relationships in Transcriptional  
777 Regulatory Networks. *Trends in Genetics*. 2003; 19(8):422–427. [http://www.sciencedirect.com/science/article/](http://www.sciencedirect.com/science/article/pii/S0168952503001756)  
778 [pii/S0168952503001756](http://www.sciencedirect.com/science/article/pii/S0168952503001756), doi: [https://doi.org/10.1016/S0168-9525\(03\)00175-6](https://doi.org/10.1016/S0168-9525(03)00175-6).
- 779 **Yu J**, Xiao J, Ren X, Lao K, Xie XS. Probing Gene Expression in Live Cells, One Protein Molecule at a Time.  
780 *Science*. 2006; 311(5767):1600–1603. <https://science.sciencemag.org/content/sci/311/5767/1600.full.pdf>, doi:  
781 [10.1126/science.1119623](https://doi.org/10.1126/science.1119623).
- 782 **Zaslaver A**, Mayo AE, Rosenberg R, Bashkin P, Sberro H, Tsalyuk M, Surette MG, Alon U. Just-in-Time Transcription  
783 Program in Metabolic Pathways. *Nature Genetics*. 2004; 36(5):486–491. <https://doi.org/10.1038/ng1348>, doi:  
784 [10.1038/ng1348](https://doi.org/10.1038/ng1348).

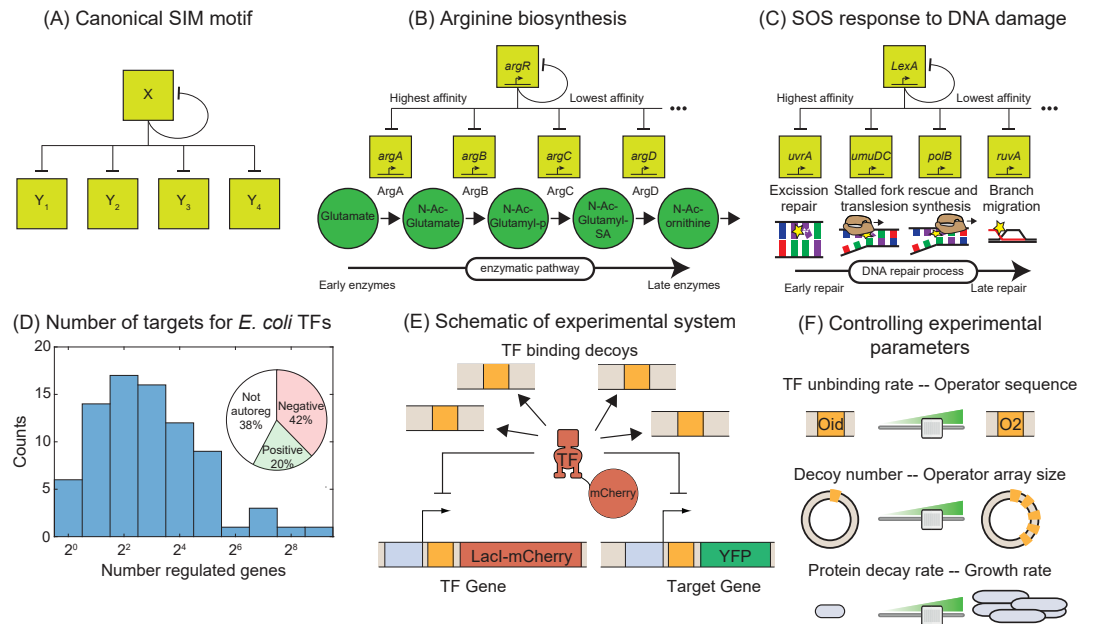


**Figure 1. Synthetic approach to exploring the negative SIM motif.** (A) Schematic of a canonical SIM motif: A single TF regulates itself and several other genes. (B and C) Examples of SIM motifs in *E. coli*. (B) ArgR is a transcriptional regulator of arginine biosynthesis. It auto-regulates itself and genes involved in different steps of arginine biosynthesis with precision in expression starting from the first enzyme of the pathway down to the last. This precise ordering is thought to originate from a corresponding ordering in TF binding affinities of the target genes. (C) LexA is the master regulator of SOS pathway and is actively degraded in response to DNA damage. LexA auto-represses itself and represses a set of other genes involved in DNA repair. In this case the early response genes have low affinity for the repressor while the late acting genes have high affinity, enabling temporal ordering of the response. (D) Histogram showing the number of known regulated genes for every TF in *E. coli*. Inset shows different modes of regulation of the TF genes. 62% of the TF genes are autoregulated with 42% negatively autoregulated and 20% positively autoregulated. (E) Schematic of the experimental model of a SIM motif used in this study. Here, Lacl-mCherry is the model TF and YFP is the protein product of the target gene. Decoys sites are used to control the network size by simulating the demand of other target genes in the SIM motif. (F) Representation of the tunable parameter space detailed in this study. We can systematically tune the TF unbinding rate, number of decoys and protein degradation rate in the experimental system and adjust these parameters accordingly in simulations.

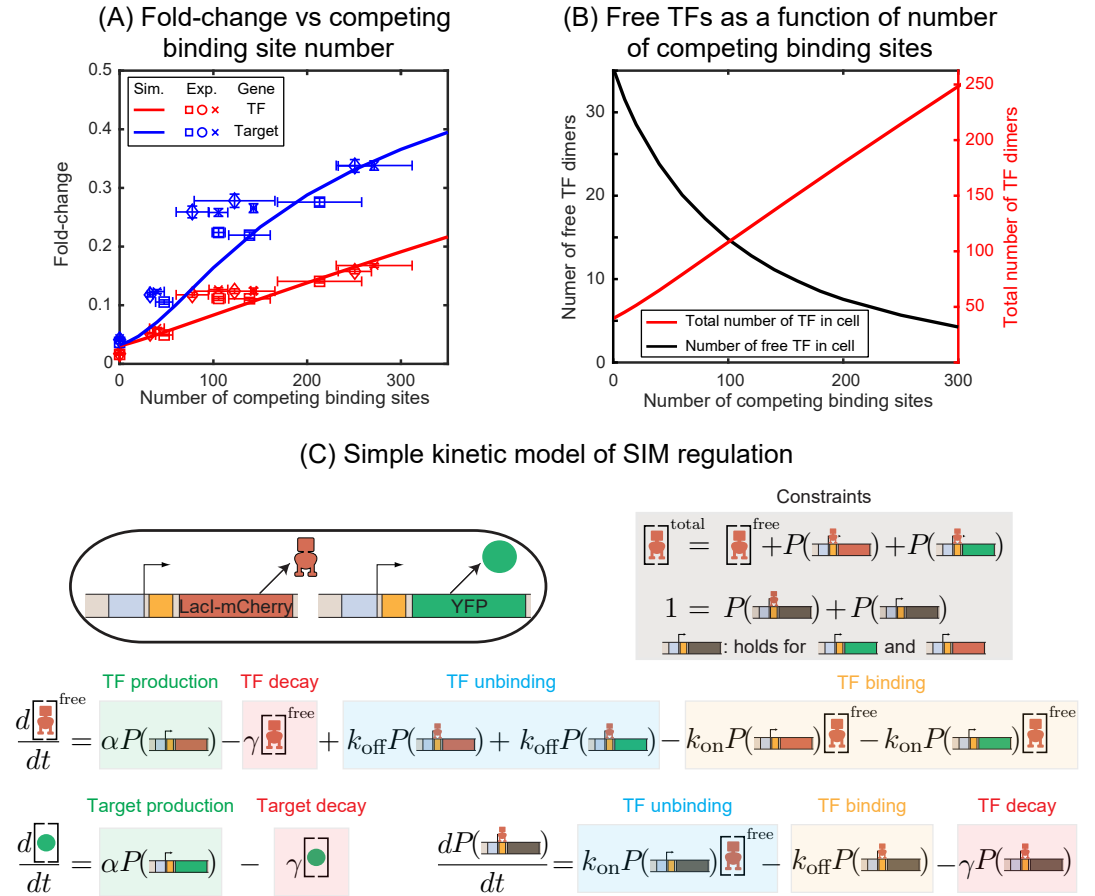


**Figure 2. Fold-change in target and TF genes with network size.** (A) Fold-change in the expression level of both the autoregulated gene (red) and the TF's target gene (blue) as a function of the number of competing binding sites present. Simulation data is shown as solid curves. Different symbols represent independent biological replicates. Each data point in y-axis is the bootstrapped mean of individual decoy strains and the error bars represent the standard deviation of bootstrapped mean. Each data point in x-axis is the mean of three technical replicates and the error bar is the corresponding standard deviation. (B) Increasing the number of competing binding sites increases the expression of both the TF (red line) and target genes by lowering the overall number of free TFs (black line). (C) Simple kinetic model describing the SIM motif using mass action equilibrium kinetics. For compactness of the figure the reactions involving the decoy binding sites, dimerization/dedimerization of TF monomers, and transcription steps are not shown. Full reactions of the model are described in Appendix 6.

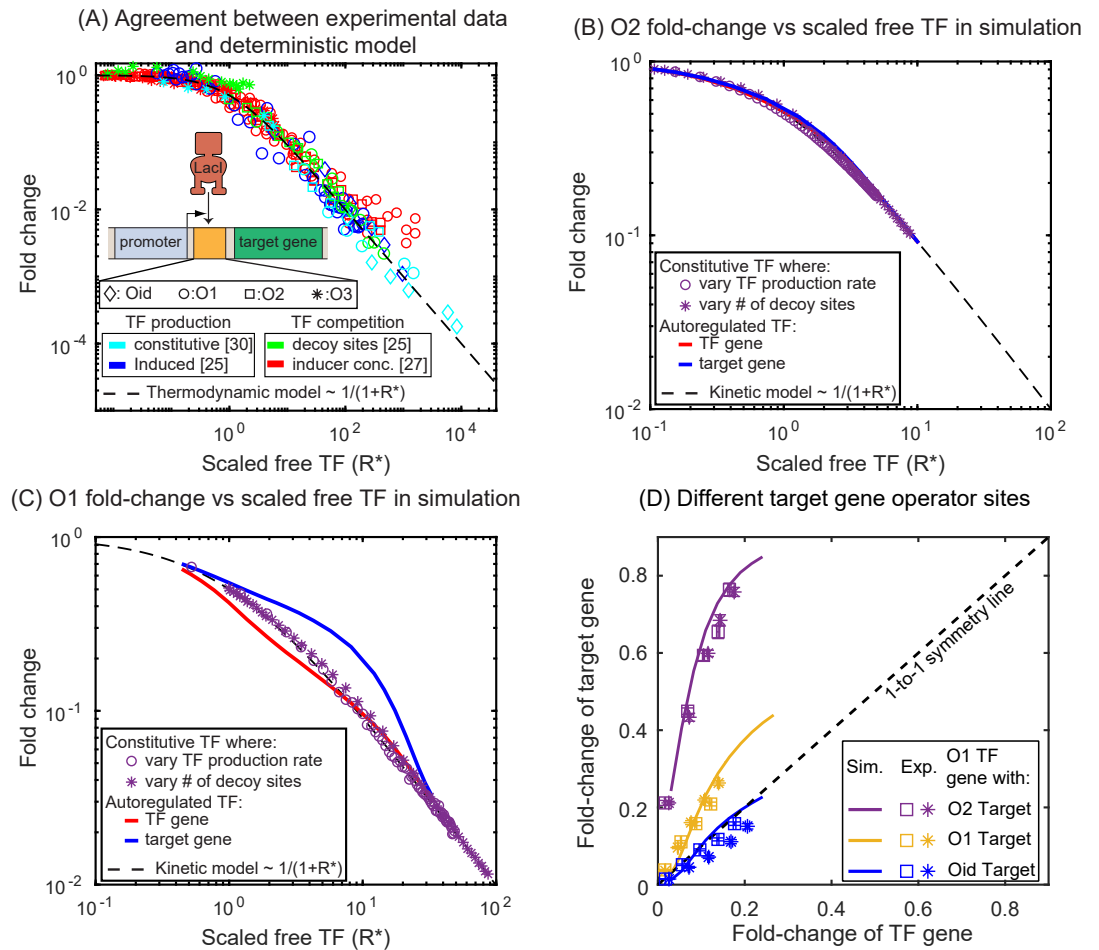


**Figure 3. Comparison of SIM motif fold-change data to deterministic model predictions.** (A) Fold-change vs scaled free TF in the thermodynamic model for a collection of simple repression data (open circles) where free TF is controlled through a diverse range of mechanisms. The data collapse to the deterministic model predictions (dashed curve). (B-C) Fold-change vs scaled free TF in simulations using the actual free TF obtained from simulation. The data for a constitutive expressed TF where free TF is varied by changing TF production rate (purple circles) or number of decoy sites (purple stars) collapses to the deterministic solution, however, the regulation of genes in the SIM motif (target: red line, TF gene: blue line) both diverge from the deterministic solution in opposing ways, giving rise not only to asymmetry but a disagreement with deterministic modeling for both genes. (D) Fold-change in the target gene versus fold-change in the TF gene. Each data point is the bootstrapped mean of fold-change in TF and target expression across hundreds of cells with a given number of competing binding sites and error bars represent the standard deviation of the bootstrapped mean. Different symbols represent independent biological replicates. In all cases the TF gene is regulated by an O1 binding sites whereas the target is regulated by (in order of weakest binding to strongest binding): O2 (purple), O1 (yellow) or Oid (blue). Simulation data is shown as solid curves.

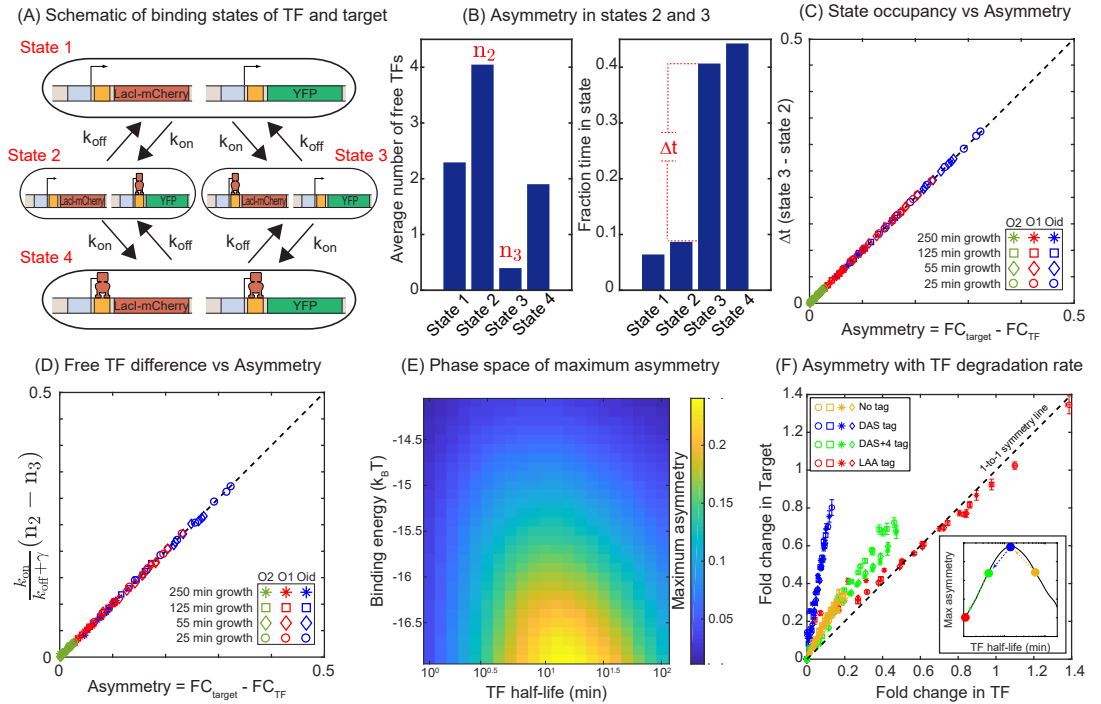


**Figure 4. Mechanism of regulatory asymmetry.** (A) Schematic of the TF-operator occupancy with their corresponding transition rates. The  $k_{on}$  for transition from state 1 to state 2 or state 3 will be identical and hence cannot account for the asymmetry. State 2 and state 3 on the other hand, will encounter a difference in the free TF concentration and hence the  $k_{on}$  for transition from one of these states to state 4 will be different; thus, accounting for the asymmetry in expression between the TF and the target. (B) Plot showing the average number of free TFs in different states and fraction of time cells spends in each of the given state in the simulation. (C) Plot showing asymmetry as a function of fractional time difference between state 2 and state 3. (D) Plot showing asymmetry as a function of difference in free TF concentration between state 3 and state 2. (E) Heat map showing the phase space of maximum asymmetry as a function of binding affinity for the TF and its half-life. (F) Tuning the TF degradation rate influences the extent of asymmetry observed in the SIM module. Yellow points corresponds to the system with no degradation tags; Blue points corresponds to degradation by a “weak” or “slow” tag (DAS tag with a rate of 0.00063 per min per enzyme); Green points corresponds to a slightly faster tag (DAS+4 with a rate of 0.0011 per min per enzyme ); Red points corresponds to a very fast tag (LAA tag with a rate of 0.21 per min per enzyme ). Different symbols represent independent biological replicates.

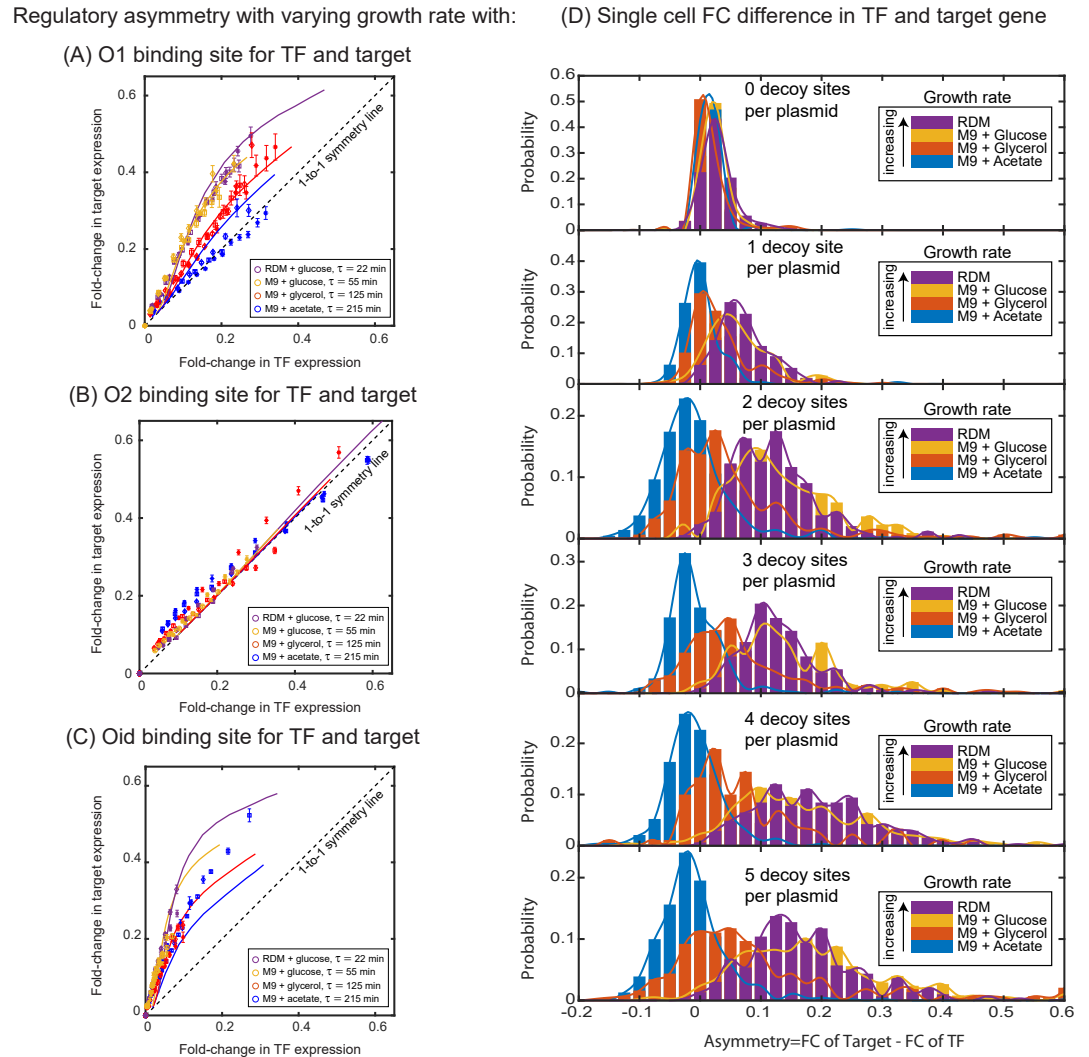


**Figure 5. Dependence of regulatory asymmetry on growth rate.** Measurement of asymmetry in different media as a function of TF binding energy: O1 (A), O2 (B), Oid (C). The division time ( $\tau$ ) is varied between 22 minutes up to 215 minutes. (A) For O1, the asymmetry decreases with slower division rates and agrees well with the simulation predictions. (B) For the weak O2 site, no asymmetry is seen at any growth rate. (C) For the strongest site Oid asymmetry is present at every growth rate although the magnitude of asymmetry still orders roughly by growth rate. Different symbols represent independent biological replicates and simulation data are shown as solid curves. (D) Histograms of single-cell asymmetry in expression of the TF and target gene regulated by O1 binding site in these 4 growth rates. Solid lines represent the interpolated distributions for better visualization of the histograms. Panels from top to bottom represent increasing the level of competition for the TF.

**Table 1.** Primers used in this study are listed below. Primers for the chromosomal integration of TF and the target are the same as described in (*Brewster et al. (2014)*). Primers to mutate the binding sites from O1 to Oid, O2 or NoO1V1 is listed below with the binding sites highlighted in yellow. Primers to introduce the degradation tags to LacI mCherry fusion protein is listed below with tag sequence highlighted in red.

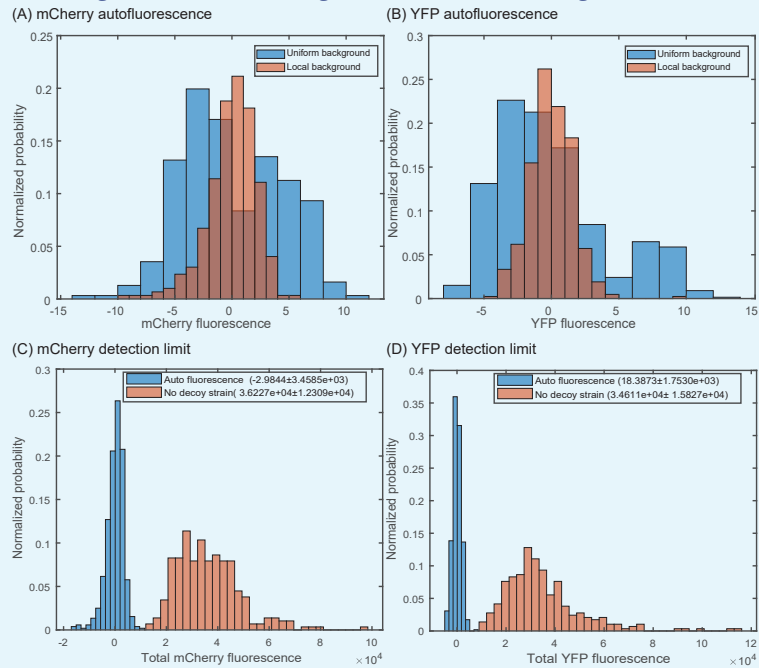
<b>Mutagenesis Primer</b>	
Oid_mutagenesis_FP	CCGGCTCGTATAATGTGTGG AATTGTGAGCGCTCACAATT GAATTCATTAAGAG
Oid_mutagenesis_RP	CTCTTAATGAATTC AATTGTGAGCGCTCACAATT CCACACATT ATACGAGCCGG
O2_mutagenesis_FP	GTGAGCGAGTAACAACC GAATTCATTAAGAGGAGAAAGGTAC
O2_mutagenesis_RP	TTGTTACTCGCTCACATT CCACACATTATACGAGCC
NoO1V1_mutagenesis_FP	GATTGTTAGCGGAGAAGAATT GAATTCATTAAGA GGAGAAAGGTACC
NoO1V1_mutagenesis_RP	AATTCTTCCGCTAACAATC CCACACATTATACGAGCCGGAAG
<b>Primers to introduce tags</b>	
ssrA_WT_FP	GC AGCAAACGACGAAAACACTACGCTTAGCAGCT TAAGCTTAA TTAGCTGAGTCTAGAGGC
ssrA_WT_RP	AGCTGCTAAAGCGTAGTTTTTCGTCGTTTGCT GCTTTGTA CAGCTCATCCATGC
DAS_FP	C AGCAAACGACGAAAACACTACGCTGATGCATCT TAAGCTTAA TAGCTGAGTCTAGAGGC
DAS_RP	AGATGCATCAGCGTAGTTTTTCGTCGTTTGCT GCTTTGTAC AGCTCATCCATGC
DASplus4_FP	GCAGCAAACGACGAAAACACTACTCTGAAAATTATGCTGATGCATCT TAAGCTTAATTAGCTGAGTCTAGAGGC
DASplus4_RP	AGATGCATCAGCATAATTTTTAGAGTAGTTTTTCGTCGTTTGCT GCTTTGTACAGCTCATCCATGC
<b>qPCR primers</b>	
qPCR_FP	GCATTTATCAGGGTTATTGTCTCAT
qPCR_RP	GGGAAATGTGCGCGGAAC

**Table 2.** Kinetic rates used in the simulations

Rates	Symbols	Value	Reference
Growth rate	$\ln 2/\gamma$	25 min (RDM) 55 min (Glucose) 125 min (Glycerol) 225 min (Acetate)	Measured experimentally
Binding of TF	$k_{on}$	0.0015 TF <sup>-1</sup> s <sup>-1</sup>	Obtained from fit
Unbinding of TF	$k_{off}$	0.00042 s <sup>-1</sup> (Oid) 0.00149 s <sup>-1</sup> (O1) 0.0167 s <sup>-1</sup> (O2)	Eqn. 1
mRNA degradation	$\gamma_m$	0.033 s <sup>-1</sup>	Obtained from fit
mRNA production	$\beta$	0.1 s <sup>-1</sup>	Obtained from fit
Translation rate	$\alpha$	0.03-0.2 s <sup>-1</sup>	Obtained from fit
Dimerization	$k_p$	1.38s <sup>-1</sup>	<i>Stamatakis and Zygorakis (2011)</i>
Monomerization	$k_m$	0.000002s <sup>-1</sup>	<i>Stamatakis and Zygorakis (2011)</i>

786 **Appendix 1**787 **Sensitivity in choosing the background values**

788 The local background of each image is subtracted from individual cells of that image, rather  
 789 than using a global average over every position. Getting a precise quantitative measurement  
 790 of fluorescence values is important especially for the tagged strains as their mCherry signal  
 791 can be only several counts above autofluorescence. The background fluorescence can be  
 792 influenced by factors such as the local thickness of the agarose pad and positional effects due  
 793 to the glass dish (which can have small local defects). As shown in **Appendix 1 Figure 1**, a  
 794 no fluorescent strain corrected using the local fluorescence (calculated by making an inverse  
 795 mask of each frame, excluding regions with cell, and calculating the mean intensity of the  
 796 background) of each frame produces a tight, symmetric distribution of cell fluorescence with  
 797 the mean centered near 0 when compared to using the mean value of no fluorescent strain.  
 798 In other words, many of the YFP or mCherry signals that appear high in the autofluorescence  
 799 samples also have higher than average backgrounds and thus accounting for this image to  
 800 image difference is important. Hence, for all experiments we have used the local background  
 801 fluorescence of each frame to correct for the autofluorescence of cells in the corresponding  
 802 frame and excluding frames with too high variation in the background fluorescence.

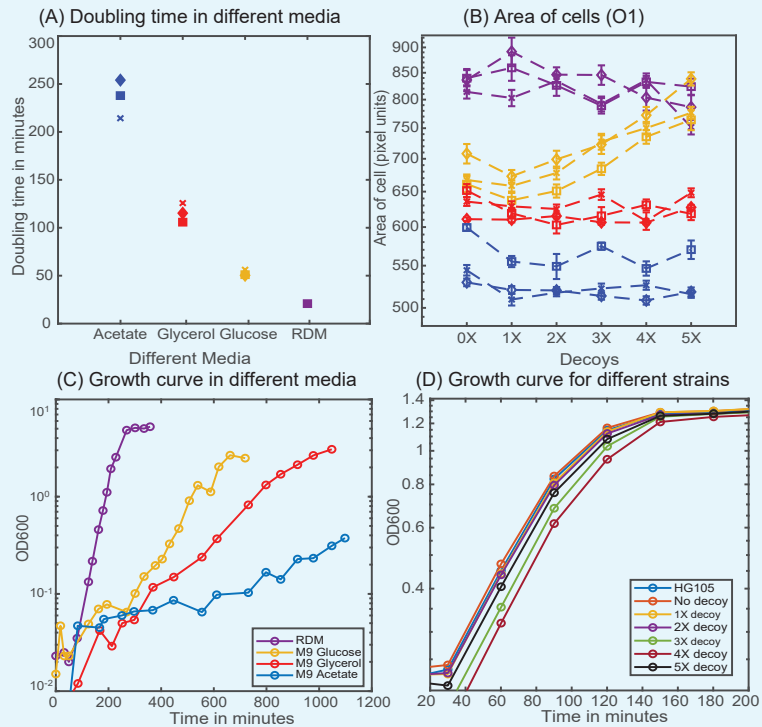


803 **Appendix 1 Figure 1. Accounting for local variation in background fluorescence.** Histogram of  
 804 single-cell autofluorescence levels of (A) mCherry or (B) YFP fluorescence in a strain without the YFP and  
 805 mCherry cassettes. The blue bars are calculated as the fluorescence level subtracted from the average  
 806 across the entire sample (9 different fields of view). The red bars are calculated by first removing the  
 807 local background fluorescence from cells at each position before subtracting the remaining signal from  
 808 the average. The wide distribution seen in the blue bars is owed largely to local differences in  
 809 background fluorescence and is removed by accounting for position-to-position variability. (C,D)  
 810 Histogram showing the minimal detection limit (in a no decoy strain) for mCherry (C) and YFP (D)  
 811 compared to an autofluorescence strain.

814 **Appendix 2**

815 **Cell growth rate in different media**

816 Cell growth rate is measured in strain HG105 growing in a 50 mL flask at 37°C and at 250 rpm.  
 817 Samples are collected at precise time points and OD600 is measured (see **Appendix 2 Figure**  
 818 **1C**). Doubling time is calculated by first interpolating the intermediate time points from the  
 819 measurements of OD600 and with the single exponential robust fit function in Matlab (see  
 820 **Appendix 2 Figure 1A**). **Appendix 2 Figure 1B** shows the scaling in cell area (measured in  
 821 pixel units) in different media in accordance with the previous literature *Jun et al. (2018)*.  
 822 Interestingly, the strain with 5X decoy plasmid has a strikingly different area (from other  
 823 strains) in glucose minimal media possibly indicating sickness due to the presence of multiple  
 824 arrays of Oid binding site. Hence, results of 5X decoy strain is excluded from the data set for  
 825 glucose minimal media.

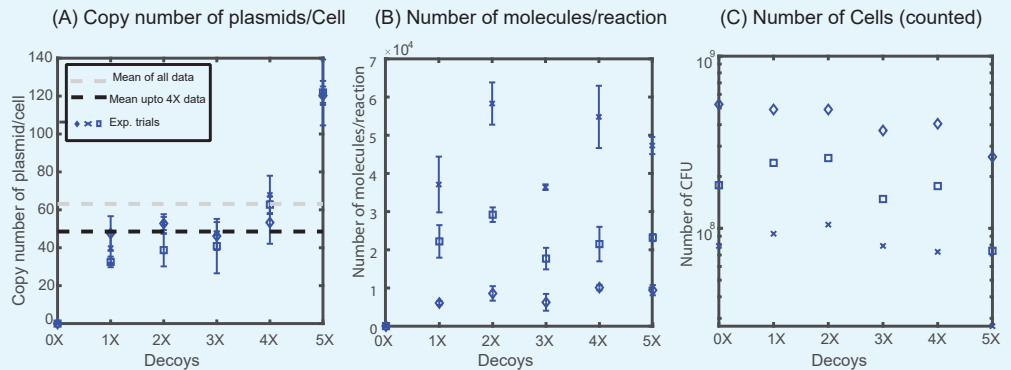


826 **Appendix 2 Figure 1. Cellular physiology in different media.** (A) Doubling time of HG105 in  
 827 different media used in this study. (B) Consistent with the literature there is a scaling of cell area in  
 828 different media in accordance with their growth rate. Strains with 4X and 5X decoys growing in glucose  
 829 minimal media have a drastically different cell area. (C) Plot showing the growth curves for the strain  
 830 HG105 grown in M9-minimal media with glucose, glycerol and acetate or in rich-defined media. (D) Plot  
 831 showing the growth curves in rich-defined media for strains carrying in different decoy plasmid. Cells  
 832 are grown in TECAN machine (maintained at 37°C) in a 96-well plate with constant shaking and  
 833 measurements are made every 30 minutes.  
 835

836 **Appendix 3**

837 **Quantification of plasmid copy number**

838 Five different variants of Oid decoy arrays (carrying 1, 2, 3, 4 and 5 binding sites for Oid,  
 839 respectively) are inserted in the intergenic region between the origin of replication and ampi-  
 840 cillin cassette of the pZE plasmid. Plasmid copy number is quantified in qPCR measurements  
 841 using primers that targets a 90 bp-intergenic region in the plasmid backbone immediately  
 842 upstream of the site of insertion of our decoy array. The total number of decoys can then  
 843 be estimated by multiplying the measured copy number of pZE plasmid backbone with  
 844 the number of binding sites in the decoy array. As shown in **Appendix 3 Figure 1A**, pZE  
 845 plasmid backbone had similar copy number in strains with different decoy arrays except  
 846 for strains carrying the 5X decoy array plasmid. Copy number of 5X-decoy array plasmid  
 847 is significantly higher when compared to strains carrying other decoy array plasmids. This  
 848 difference is primarily due to a reduced CFU/mL obtained (see **Appendix 3 Figure 1C**) for  
 849 strains carrying the 5X decoy arrays; the number of molecules of plasmid per reaction is  
 850 uniform across different strains (see **Appendix 3 Figure 1B**). It is not clear if this is due to  
 851 this sample actually containing less cells or if it is due to a reduced ability to recover and se-  
 852 parate these cells (which tend to clump and stick more in microscopy imaging) in the plating  
 853 assay. This may lead to over-prediction of the copy number of 5X decoy plasmid. Hence,  
 854 we excluded the 5X-decoy plasmid data in Figure 2A. The average ( $\pm$  standard deviation)  
 855 number of decoy binding arrays in different strains are:  $39\pm 8$ ,  $96\pm 17$ ,  $134\pm 25$ ,  $245\pm 40$ , and  
 856  $607\pm 47$ , respectively.



857 **Appendix 3 Figure 1. Quantification of plasmid copy number.** (A) Copy number of decoy array  
 858 plasmids measured in M9-Glucose minimal media. (B) Number of molecules obtained per qPCR  
 859 reaction remains constant across different decoy strains (1X, 2X, 3X, 4X, 5X). (C) Number of Colony  
 860 Forming Units (CFU) per mL used to normalize the number of molecules to account for the copy  
 861 number of plasmids per cell.  
 862

864 **Appendix 4**865 **Constitutive values for the autoregulatory gene**

866 To compare expression levels between the TF and the target genes, we wish to compare  
867 fold-change as an “apples-to-apples” comparison of the regulation of each gene. To calculate  
868 fold-change we must know the constitutive expression of the gene, *i.e.* how much expression  
869 is seen in the absence of regulation by TF. In simulation, this is simple to calculate because  
870 we can remove any reactions that include TF binding. Experimentally, calculating constitutive  
871 expression for the target gene is also relatively straight-forward; we delete the gene express-  
872 ing LacI-mCherry and measure the same construct in the absence of TF. However, measuring  
873 constitutive expression experimentally for an autoregulating gene was more challenging.  
874 There are many possible strategies, but all of them come with some complication. In short,  
875 we attempted 3 different strategies which included: 1) IPTG induction (with or without the  
876 addition of decoys), 2) mutated LacI to ablate specific binding, 3) mutated binding site se-  
877 quences (which has the complication that the site is centered at +11 and thus is both close  
878 to the promoter and present on the transcript, see **Appendix 4 Figure 1A**). In the end, we  
879 identified one mutated site (NoO1V1) which faithfully preserved constitutive expression of  
880 the target gene in all media studied. Unfortunately, we were not able to find corresponding  
881 mutated sites that reproduced expression of promoters bearing O2 or Oid binding sites. As  
882 such, for data using those binding sites on the TF gene we have an unknown scaling factor  
883 between the x- and y-axis in the fold-change versus fold-change plots which we determine  
884 by fitting the glucose data to our simulations (and then hold constant for all other data sets).  
885 In the following sections we discuss techniques we tried.

886 *Allosteric induction with IPTG to achieve constitutive expression*

887 One way to obtain the constitutive values is to exploit the property of the LacI to become less  
888 active when bound to small molecules like IPTG. Previous studies indicate that even with the  
889 use of IPTG, expression from a stronger binding site (like Oid) cannot be fully rescued when  
890 the repressor copy number is high *Razo-Mejia et al. (2018)*. In our experiments, we observed  
891 this phenomenon as well. As shown in **Appendix 4 Figure 1C-E**, for most strains expressing  
892 the TF, the expression of the target could not be fully rescued with 2.5mM IPTG and decoys.  
893 Further increase in IPTG concentration (to up to 10mM) did not help in increasing the target  
894 expression. Hence, allosteric induction with IPTG could not serve as a right constitutive value  
895 for our system.

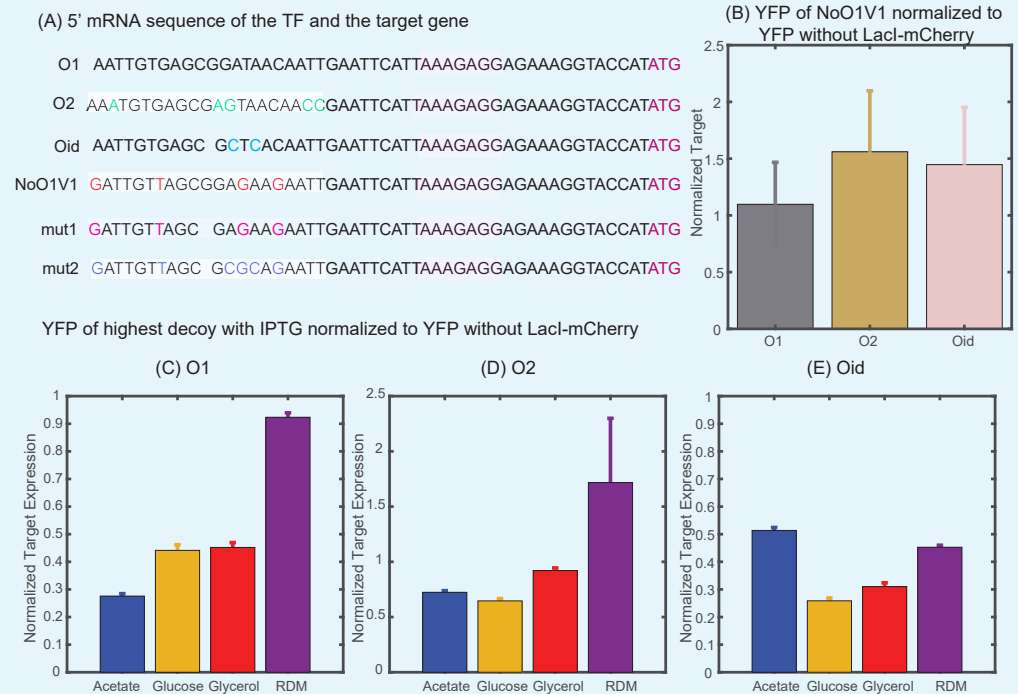
896 *Use of LacI with mutated DNA recognition domains*

897 We constructed a mutant protein by deleting 10 amino acids (from amino acid 60 to amino  
898 acid 70) in the DNA binding domain of LacI. This mutant helped to completely restore the  
899 target expression. However, the mCherry level of strains with the mutated LacI-mCherry were  
900 significantly lower than the mCherry level of strains with the functional LacI-mCherry. Since,  
901 we would expect the expression of the non-functional TF to be higher than the functional, we  
902 reason that this did not provide an accurate estimate of the constitutive mCherry level in the  
903 LacI-mCherry strain. This discrepancy may originate from many possible sources such as a  
904 change to the stability of the mRNA/protein or a possible alteration to the spectral property  
905 of mCherry (which is directly fused to LacI). In the end we were unable to find a suitable LacI  
906 mutant without this feature.

907  
908  
909  
910  
911  
912  
913  
914  
915  
916  
917  
918

*Use of binding sequence insensitive to LacI*

Oehler *et al.* 1994 has reported inactivated O1 site (NoO1V1) that has close consensus to O1 binding sequence but does not allow LacI binding. We verified that the expression of YFP from the promoter with NoO1V1 is comparable to the expression of YFP from O1 regulated promoter (in the absence of any LacI) but is lower than the expression from O2 and Oid regulated promoters (**Appendix 4 Figure 1B**). Although expression alone does not guarantee that all intermediate steps are precisely the same, we believe this construct gives accurate measurements of constitutive expression for the TF and target genes. We used TF and target with NoO1V1 binding sequence as our constitutive strain to normalize expression from any O1 regulated genes in our experiments. We also tried other forms of mutations on the NoO1V1 binding site (**Appendix 4 Figure 1A**) in order to obtain mutants that relieves *lacI* repression and restore expression of Oid or O2 sequence but with no success.



919  
920  
921  
922  
923  
924  
925  
926  
927  
928  
929

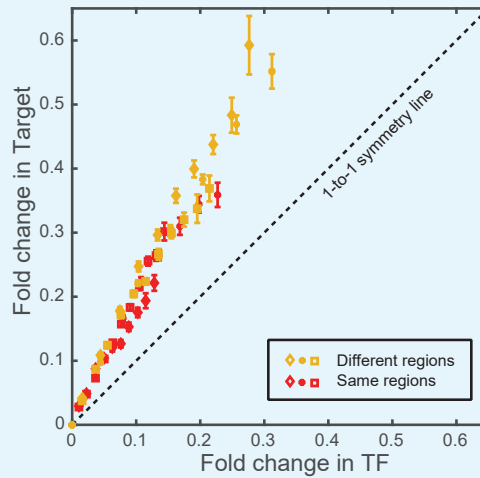
**Appendix 4 Figure 1. Determining constitutive expression of YFP and mCherry.** (A) 5' mRNA sequence of the TF and the target genes. The binding site for the TF is carried in the mRNA sequence and is highlighted in shaded dark grey boxes with base changes for different binding sites coded in multicolor. mut1 and mut2 are the two variant binding sites that are designed with mutations similar to NoO1V1 but with Oid site length. However, such changes do not achieve constitutive unregulated expression similar to O2 or Oid. (B) Plot showing YFP expressed from NoO1V1 regulated promoter normalized to YFP expressed from promoter regulated with O1, O2 or Oid. (C-E) Plot showing the effect of 2.5mM IPTG in relieving YFP expression from O1 (C), O2 (D) or Oid. (E) regulated promoter and with 5X decoy plasmids. As indicated in the plot IPTG is not sufficient to restore complete expression of YFP in different media and hence cannot be used as a measure of constitutive expression.

931 **Appendix 5**

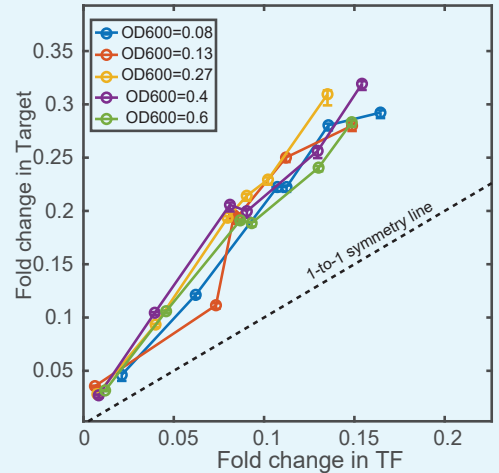
932 **Copy number difference and Diffusion limitation of TF**

933 Copy number variation of genes along the long axis of the chromosome and the diffusion  
 934 limitation of LacI-mCherry could be suggested as a significant contributor to the asymmetry  
 935 between TF and the target. *E. coli* can initiate multiple replication events (depending on  
 936 the division rate in the given media) and hence different genes along the chromosome will  
 937 experience a different copy number in a given time. For instance, *E. coli* growing in RDM  
 938 (with a division rate of 22 minutes) will have a copy number of 4 at the *ycbN* locus (where the  
 939 TF gene is integrated) and a copy number of 3.6 at the *galK* locus (where the target gene is  
 940 integrated) as described by Cooper *et al.* **Cooper and Helmstetter (1968)**. We believe that  
 941 the use of fold-change as the measurement of expression helps to reduce the influence of  
 942 copy number effects (since both the regulated and unregulated measurements have the  
 943 same copy number). However, the effects may not be linear and LacI has been shown to  
 944 suffer from diffusion limitation from its origin of synthesis **Kuhlman and Cox (2012)**. Hence,  
 945 we tested our system by placing the TF and the target genes integrated next to each other  
 946 at the *gspI* locus. As evident from **Appendix 5 Figure 1**, there is no significant contribution  
 947 of the copy number difference between TF and target or diffusion limitation of TF on the  
 948 phenomenon of asymmetry observed in our negatively-autoregulated SIM motif.

(A) Copy number of TF and target



(B) Asymmetry as a function of OD600



949 **Appendix 5 Figure 1. Effect of copy number difference on asymmetry.** Comparison of asymmetry  
 950 in strain where the TF and the target genes are located either at two different regions of the  
 951 chromosome (*ycbN* for TF and *galK* for target, shown in yellow data points)) or when it is present  
 952 together in the chromosome (at the *gspI* locus, shown in red data points). (B) Plot showing the  
 953 measurement of asymmetry in glucose-minimal media at different optical density (OD600) in the  
 954 exponential phase.

957 **Appendix 6**958 **Deterministic solution**

959 Using the assumptions of equilibrium mass-action kinetics, the deterministic counterpart of  
 960 the negative autoregulation system described in the main text and **Appendix 6 Figure 2A**  
 961 can be written as

$$\begin{aligned}
 \frac{dX}{dt} &= \alpha m_x - \gamma X + 2k_m R - 2k_p X^2, \\
 \frac{dR}{dt} &= -k_m R + k_p X^2 - \gamma R - k_{on} R P_{fx} - k_{on} R P_{fy} - k_{on} R N_f + k_{off,x}(1 - P_{fx}) \\
 &\quad + k_{off,y}(1 - P_{fy}) + k_{off,d}(N - N_f), \\
 \frac{dY}{dt} &= \alpha m_y - \gamma Y, \\
 \frac{dP_{fx}}{dt} &= -k_{on} R P_{fx} + (k_{off,x} + \gamma)(1 - P_{fx}), \\
 \frac{dP_{fy}}{dt} &= -k_{on} R P_{fy} + (k_{off,y} + \gamma)(1 - P_{fy}), \\
 \frac{dN_f}{dt} &= -k_{on} R N_f + (k_{off,d} + \gamma)(N - N_f), \\
 \frac{dm_x}{dt} &= \beta P_{fx} - \gamma_m m_x, \\
 \frac{dm_y}{dt} &= \beta P_{fy} - \gamma_m m_y.
 \end{aligned} \tag{A6-1}$$

966 Here,  $X$  is the concentration of free TF monomer,  $Y$  is the concentration of target protein,  
 967 and  $R$  is the concentration of TF dimer.  $m_x, m_y, P_{fx}(P_{ox}), P_{fy}(P_{oy}), N$ , and  $N_f(N_o)$  are TF mRNA,  
 968 target mRNA, free (bound) TF-promoter, free (bound) target-promoter, total concentration  
 969 of decoy sites, and concentration of free (bound) decoy sites, respectively. Inherent in the  
 970 equations are the assumptions of the conservation for the concentration of binding sites,  
 971 i.e.  $P_{fx} + P_{ox} = 1$ ,  $P_{fy} + P_{oy} = 1$ , and  $N_f + N_o = N$ . The right hand side of the equations can be  
 972 set to zero to obtain the steady state values for all the components.

$$\begin{aligned}
 P_{fx} &= \frac{k_{off,x} + \gamma}{k_{on} R + k_{off,x} + \gamma} = \frac{1}{1 + \sigma_1 R}, \\
 P_{fy} &= \frac{k_{off,y} + \gamma}{k_{on} R + k_{off,y} + \gamma} = \frac{1}{1 + \sigma_2 R}, \\
 N_f &= \frac{N(k_{off,d} + \gamma)}{k_{on} R + k_{off,d} + \gamma} = \frac{N}{1 + \sigma_3 R}, \\
 m_x &= \frac{\beta}{\gamma_m} P_{fx}, \\
 m_y &= \frac{\beta}{\gamma_m} P_{fy}, \\
 0 &= \alpha m_x - \gamma X + 2k_m R - 2k_p X^2, \\
 0 &= -k_m R + k_p X^2 - \gamma(R + P_{ox} + P_{oy} + N_o) \\
 Y &= \frac{\alpha \beta}{\gamma \gamma_m} P_{fy} = \frac{\alpha \beta}{\gamma \gamma_m} \frac{1}{1 + \sigma_2 R},
 \end{aligned} \tag{A6-2}$$

977 where  $\sigma_i = k_{on}/(k_{off,i} + \gamma)$ . The concentration of total TF protein can be expressed as a  
 978 sum of free TF monomer, TF dimer bound to each promoter, and TF dimers bound to the  
 979 decoys sites

980  
981  
982  
983  
984  
985  
  
986  
987  
988  
989  
  
990  
991  
992  
993  
994  
995  
996  
997  
998  
999  
1000  
1001  
1002  
  
1003  
1004  
1005  
1006  
1007  
1008  
1009  
1010  
1011  
1012  
1014

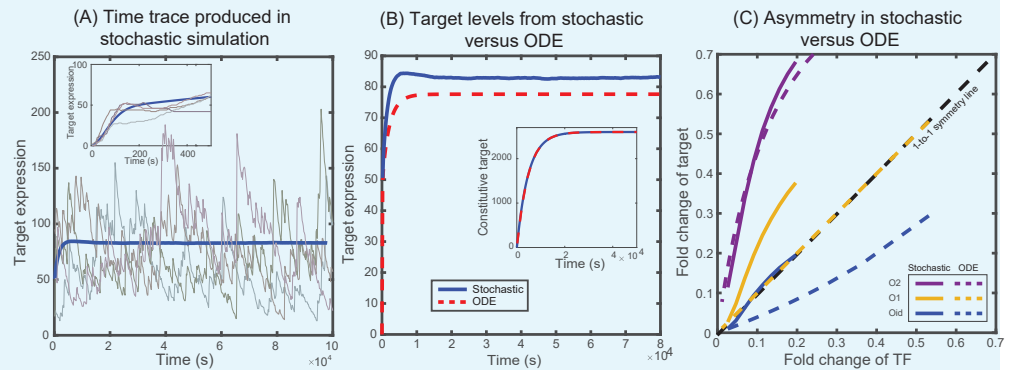
$$\begin{aligned}
 X_{\text{Total}} &= X + 2(R + P_{\text{ox}} + P_{\text{oy}} + N_o), \\
 &= \frac{\alpha}{\gamma} m_x, \\
 &= \frac{\alpha\beta}{\gamma\gamma_m} \frac{1}{1 + \sigma_1 R}.
 \end{aligned}
 \tag{A6-3}$$

The fold-change of the TF and target expression, thus can be obtained by dividing  $X_{\text{Total}}$  and  $Y$  with the constitutive expression, i.e.,  $\alpha\beta/\gamma\gamma_m$  which yields,

$$\text{FC}_{\text{TF}} = \frac{1}{1 + \sigma_1 R} = \frac{1}{1 + \frac{k_{\text{on}}}{k_{\text{off},x} + \gamma} R},
 \tag{A6-4}$$

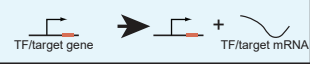











$$\text{FC}_{\text{Target}} = \frac{1}{1 + \sigma_2 R} = \frac{1}{1 + \frac{k_{\text{on}}}{k_{\text{off},y} + \gamma} R}.
 \tag{A6-5}$$

It is worth noting that both TF and target protein follows  $1/(1+R^*)$ , where  $R^* = Rk_{\text{on}}/(k_{\text{off}} + \gamma)$  is the reduced free TF concentration, which is equivalent to the thermodynamic solution *Weinert et al. (2014)*. When the unbinding rates of TF and target are identical, each of them follow the same fold-change curve irrespective of the competition from other decoy sites. In **Appendix 6 Figure 1C**, we plot the fold-change for TF and target with  $k_{\text{off},x}$  corresponding to O1 binding site and  $k_{\text{off},y}$  corresponding to O1 (yellow), O2 (purple), and Oid (blue). It can be seen from the figure that when the off-rates are identical the fold-change curve follows one-to-one line showing no asymmetry which is in contrast with the results obtained using stochastic simulations and experimental results. Furthermore, both the transient and steady state behavior of mean fold-change of TF and target obtained from deterministic solution deviate from the stochastic behavior (see **Appendix 6 Figure 1B**). Importantly, when autoregulation is removed from the simulation, the deterministic and stochastic solutions agree precisely (**Appendix 6 Figure 1B inset**).

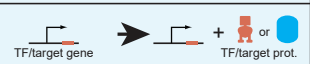






**Appendix 6 Figure 1. Solutions from stochastic simulation and from deterministic ODEs. (A)** Representative time traces of target expression in individual cells (grey shades) from stochastic simulations. Blue solid line represents the mean behavior averaged over  $5 \times 10^4$  iterations. Inset shows the transient behavior. **(B)** Plot showing the average target expression in the negative SIM motif from stochastic simulations (solid line) and from solving deterministic ODEs (dashed line). Inset shows that when regulation is removed the average levels are identical for stochastic and deterministic models. **(C)** Plot showing the asymmetry between TF and target expression from using either stochastic simulation (solid lines) or solving deterministic ODEs (dashed lines). The TF is always regulated by O1 binding site whereas the target is regulated by O1 (yellow), O2 (purple) or Oid (blue) binding sites. The black dashed line represents line of no asymmetry.

(A) Full model

Schematic reaction	Stochastic chemical reaction	Deterministic rate
	$m_{TF(Target)} \xrightarrow{\beta} m_{TF(Target)} + 1$	$\beta P_{I_x(f_y)}$
	$m_{TF} \xrightarrow{\alpha} m_{TF} + X$	$\alpha m_x$
	$m_{Target} \xrightarrow{\alpha} m_{Target} + Y$	$\alpha m_y$
	$X + X \xrightarrow{k_p} Z$	$k_p X^2$
	$Z \xrightarrow{k_m} X + X$	$k_m Z$
	$Z + P_{TF(Target)} \xrightarrow{k_{on}} ZP_{TF(Target)}$	$k_{on} Z P_{I_x(f_y)}$
	$ZP_{TF(Target)} \xrightarrow{k_{off,TF(Target)}} Z + P_{TF(Target)}$	$k_{off,x(off,y)}(1 - P_{I_x(f_y)})$
	$Z + N \xrightarrow{k_{on}} ZN$	$k_{on} Z N_f$
	$ZN \xrightarrow{k_{off,Decoy}} Z + N$	$k_{off,d}(N - N_f)$
	$m_{TF(Target)} \xrightarrow{\gamma_m} m_{TF(Target)}$	$\gamma_m m_x(y)$
	$X, Y, Z \xrightarrow{\gamma} \phi$	$\gamma X$ or $\gamma Y$ or $\gamma Z$
	$ZP_{TF(Target)} \xrightarrow{\gamma} P_{TF(Target)}$ or $ZN \xrightarrow{\gamma} N$	$\gamma(1 - P_{I_x(f_y)})$ or $\gamma(N - N_f)$

(B) Minimal model to demonstrate asymmetry

Schematic reaction	Stochastic chemical reaction	Deterministic rate
	$P_{TF(Target)} \xrightarrow{\alpha} P_{TF(Target)} + X(Y)$	$\alpha P_{I_x(f_y)}$
	$X + P_{TF(Target)} \xrightarrow{k_{on}} X P_{TF(Target)}$	$k_{on} X P_{I_x(f_y)}$
	$X P_{TF(Target)} \xrightarrow{k_{off}} X + P_{TF(Target)}$	$k_{off}(1 - P_{I_x(f_y)})$
	$X, Y \xrightarrow{\gamma} \phi$	$\gamma X$ or $\gamma Y$
	$X P_{TF(Target)} \xrightarrow{\gamma} P_{TF(Target)}$	$\gamma(1 - P_{I_x(f_y)})$

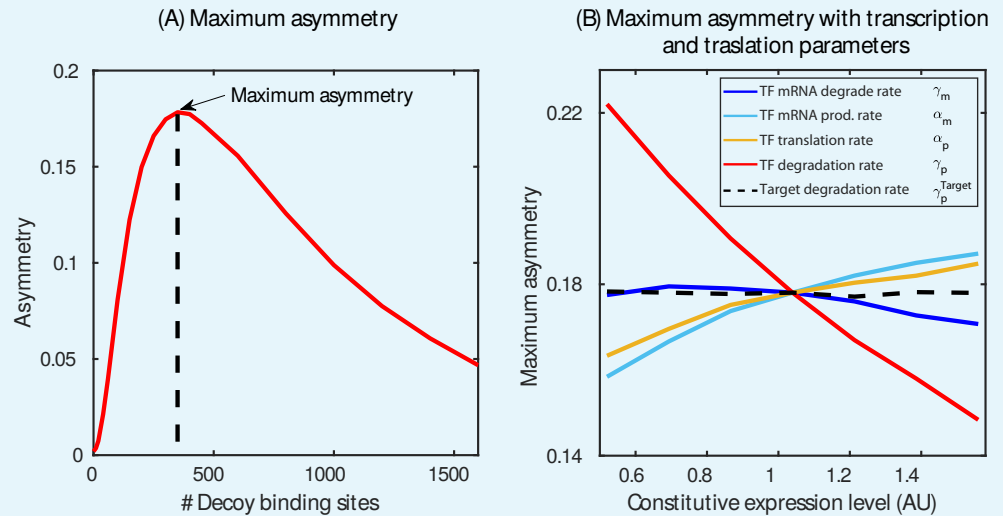
1015  
1016  
1018

Appendix 6 Figure 2. List of reactions used in the (A) stochastic model and (B) in the minimal model.

1019 **Appendix 7**

1020 **Maximum asymmetry**

1021 The asymmetry in regulation (defined as  $FC_{TF} - FC_{Target}$ ) is a function of all the rates describing  
 1022 the system and number of decoy binding sites. For a given set of rates ( $k_{on}, k_{off}, \gamma, \gamma_m$ ) as  
 1023 the decoy number is varied the asymmetry first increases, attains a maximum and then  
 1024 approaches zero for infinite number of decoy binding sites (see **Appendix 7 Figure 1**). The  
 1025 maximum asymmetry for a given set of rates is this peak asymmetry observed as decoy  
 1026 number is varied. In the manuscript we show a heatmap (Fig. **3E**) to emphasize how this  
 1027 maximum asymmetry depends on the two crucial rate parameters, off-rate of the binding  
 1028 sites ( $k_{off}$  or equivalently binding affinity, since in our model  $k_{on}$  is kept constant) and the  
 1029 degradation of TF molecules ( $\gamma$ ).



1030 **Appendix 7 Figure 1. Determination of maximum asymmetry.** (A) Maximum asymmetry in  
 1031 simulation is computed by plotting the asymmetry, difference in fold-change between target and TF,  
 1032 versus number of decoy binding sites in SIM motif. The peak of this asymmetry corresponds to the  
 1033 maximum asymmetry. (B) Exploring the model parameters of the TF (mRNA production and  
 1034 degradation; protein production and degradation) that could influence the asymmetry between the TF  
 1035 and the target. Tuning the protein degradation rate (red line) has the maximum influence on the  
 1036 asymmetry between the TF and its target gene.  
 1038

1039 **Appendix 8**1040 **A minimal model of an autoregulatory gene and a single target gene**

1041 The full model in **Appendix 6** contains many reactions that are included to more faithfully  
 1042 mirror the biological system we are modeling. However, not all of these reactions are  
 1043 necessary to observe the phenomenon of asymmetry which we describe in this manuscript.  
 1044 In this section, we present a reduced model of the extended model of transcription described  
 1045 in Materials and methods to show that the asymmetry in TF and target expression stems  
 1046 from the network architecture and not due to the intermediate steps of transcription and  
 1047 the presence of excess decoy binding sites. We consider an autoregulatory gene whose  
 1048 protein product  $X$  inhibits its own expression and also represses a single target gene with  
 1049 protein product  $Y$ . To reduce the complexity, the protein is made directly from the gene with  
 1050 no intermediates (eliminating translation rates and mRNA decay rates). In this system the  
 1051 TF,  $X$ , acts as a monomer and binds to its own gene with rate  $k_{\text{on}}$  and unbinds with rate  $k_{\text{off}}$ .  
 1052 Similarly, the TF ( $X$ ) binds and unbinds from the target gene with the same rates. Both the  
 1053 TF gene and target gene in free state (not bound with TF) produces their protein with rate  
 1054  $\alpha$  which degrades with rate  $\gamma$  (dilution through cell division). The reactions describing this  
 1055 reduced model are listed in **Appendix 6 Figure 2B**. We implement the simulations using  
 1056 stochastic simulation algorithms as described in Materials and Methods section.

1057 Next, we write a set of deterministic coupled ODEs corresponding to the reactions  
 1058 described above which is given by

$$\begin{aligned}
 \frac{dX}{dt} &= \alpha P_{\text{fx}} - \gamma X - k_{\text{on}} X P_{\text{fx}} - k_{\text{on}} X P_{\text{fy}} + k_{\text{off}}(1 - P_{\text{fx}}) + k_{\text{off}}(1 - P_{\text{fy}}), \\
 \frac{dY}{dt} &= \alpha P_{\text{fy}} - \gamma Y, \\
 \frac{dP_{\text{fx}}}{dt} &= -k_{\text{on}} X P_{\text{fx}} + (k_{\text{off}} + \gamma)(1 - P_{\text{fx}}), \\
 \frac{dP_{\text{fy}}}{dt} &= -k_{\text{on}} X P_{\text{fy}} + (k_{\text{off}} + \gamma)(1 - P_{\text{fy}}).
 \end{aligned}
 \tag{A8-1}$$

1063 Here,  $X$  is the concentration of free TF and  $Y$  is the concentration of target protein.  
 1064  $P_{\text{fx}}$  ( $P_{\text{ox}}$ ) and  $P_{\text{fy}}$  ( $P_{\text{oy}}$ ) are free (bound) TF-promoter, free (bound) target-promoter, respectively.  
 1065 Inherent in the equations are the assumptions of the conservation for the concentration  
 1066 of binding sites, i.e.  $P_{\text{fx}} + P_{\text{ox}} = 1$ ,  $P_{\text{fy}} + P_{\text{oy}} = 1$ . To obtain the steady state values of TF and  
 1067 target expression the right hand side of the equations is set to zero which yield

$$\begin{aligned}
 P_{\text{fx}} &= \frac{k_{\text{off}} + \gamma}{k_{\text{on}} X + k_{\text{off}} + \gamma} = \frac{1}{1 + \sigma X}, \\
 P_{\text{fy}} &= \frac{k_{\text{off}} + \gamma}{k_{\text{on}} X + k_{\text{off}} + \gamma} = \frac{1}{1 + \sigma X}, \\
 X &= \frac{\alpha}{\gamma} P_{\text{fx}} - P_{\text{ox}} - P_{\text{oy}}, \\
 Y &= \frac{\alpha}{\gamma} P_{\text{fy}} = \frac{\alpha}{\gamma} \frac{1}{1 + \sigma X},
 \end{aligned}
 \tag{A8-2}$$

where  $\sigma = k_{\text{on}}/(k_{\text{off}} + \gamma)$ . Total TF concentration,  $X_{\text{Total}}$ , can be expressed as the sum of

1072

1073

free TF and TFs bound to each promoter

1074

1075

1076

1077

$$\begin{aligned}
 X_{\text{Total}} &= X + P_{\text{ox}} + P_{\text{oy}} \\
 &= \frac{\alpha}{\gamma} P_{\text{fx}} \\
 &= \frac{\alpha}{\gamma} \frac{1}{1 + \sigma X}.
 \end{aligned}
 \tag{A8-3}$$

1078

1079

The fold-change of the TF and target expression, thus can be obtained by dividing  $X_{\text{Total}}$  and  $Y$  by the constitutive expression, *i.e.* without any regulation,  $C_0 = \alpha/\gamma$  which yields,

1080

1081

1082

1083

$$\text{FC}_{\text{TF}} = \frac{1}{1 + \sigma X} = \frac{1}{1 + \frac{k_{\text{on}}}{k_{\text{off}} + \gamma} X},
 \tag{A8-4}$$

$$\text{FC}_{\text{Target}} = \frac{1}{1 + \sigma X} = \frac{1}{1 + \frac{k_{\text{on}}}{k_{\text{off}} + \gamma} X}.
 \tag{A8-5}$$

1084

1085

1086

1087

1088

As was shown previously in section **Appendix 6**, both TF and target protein follows  $1/(1 + \sigma X)$  and show no asymmetry in regulation.

Furthermore, solving Eqn. A8-2 we get the free TF expression as,

1089

1090

$$X = \frac{-1 - 2\sigma + \sqrt{(1 + 2\sigma)^2 + 4C_0\sigma}}{2\sigma}.
 \tag{A8-6}$$

1091 **Appendix 9**1092 **Chemical master equation (CME) for the minimal model**

1093 The chemical master equation governing the dynamics of the expression for TF and target  
 1094 gene for the minimal model discussed in **Appendix 8** (also shown in **Appendix 6 Figure 2B**)  
 1095 is given by

$$\begin{aligned}
 \frac{dP_{00}(n, m, t)}{dt} &= \alpha \left[ P_{00}(n-1, m, t) - P_{00}(n, m, t) + P_{00}(n, m-1, t) - P_{00}(n, m, t) \right] \\
 &+ \gamma \left[ (n+1)P_{00}(n+1, m, t) - nP_{00}(n, m, t) + (m+1)P_{00}(n, m+1, t) \right. \\
 &- mP_{00}(n, m, t) + P_{01}(n, m, t) + P_{10}(n, m, t) \left. \right] + k_{\text{off}} \left[ P_{01}(n-1, m, t) \right. \\
 &+ P_{10}(n-1, m, t) \left. \right] - 2k_{\text{on}}nP_{00}(n, m, t), \\
 \frac{dP_{01}(n, m, t)}{dt} &= \alpha \left[ P_{01}(n-1, m, t) - P_{01}(n, m, t) \right] + \gamma \left[ (n+1)P_{01}(n+1, m, t) \right. \\
 &- nP_{01}(n, m, t) + (m+1)P_{01}(n, m+1, t) - mP_{01}(n, m, t) \\
 &+ P_{11}(n, m, t) - P_{01}(n, m, t) \left. \right] + k_{\text{off}} \left[ P_{11}(n-1, m, t) - P_{01}(n, m, t) \right] \\
 &+ k_{\text{on}} \left[ (n+1)P_{00}(n+1, m, t) - nP_{01}(n, m, t) \right], \\
 \frac{dP_{10}(n, m, t)}{dt} &= \alpha \left[ P_{10}(n, m-1, t) - P_{10}(n, m, t) \right] + \gamma \left[ (n+1)P_{10}(n+1, m, t) \right. \\
 &- nP_{10}(n, m, t) + (m+1)P_{10}(n, m+1, t) - mP_{10}(n, m, t) \\
 &+ P_{11}(n, m, t) - P_{10}(n, m, t) \left. \right] + k_{\text{off}} \left[ P_{11}(n-1, m, t) - P_{10}(n, m, t) \right] \\
 &+ k_{\text{on}} \left[ (n+1)P_{00}(n+1, m, t) - nP_{10}(n, m, t) \right], \\
 \frac{dP_{11}(n, m, t)}{dt} &= \gamma \left[ (n+1)P_{11}(n+1, m, t) - nP_{11}(n, m, t) + (m+1)P_{11}(n, m+1, t) \right. \\
 &- mP_{11}(n, m, t) - 2P_{11}(n, m, t) \left. \right] - 2k_{\text{off}}P_{11}(n, m, t) + \\
 &k_{\text{on}} \left[ (n+1)P_{01}(n+1, m, t) + (n+1)P_{10}(n+1, m, t) \right],
 \end{aligned} \tag{A9-1}$$

1100 Here  $P_{ij}(n, m, t)$  is the probability of having  $n$  TF protein and  $m$  target protein at any instant  
 1101 of time  $t$  in the state  $(i, j)$ .  $i$  and  $j$  denotes the occupancy of the TF promoter and target  
 1102 promoter, respectively. A value of 0 indicates that the promoter of TF/target gene is occupied  
 1103 by a TF. A value of 1, similarly indicates a promoter which is free to express.

1104 Summing Eqn. A9-1 over all values of  $(m, n)$  we get the rate equation for occupancy  
 1105 defined as  $S_{ij} = \sum_{n,m=0}^{\infty} P_{ij}$  in each state

$$\begin{aligned}
 \frac{dS_{00}}{dt} &= (\gamma + k_{\text{off}})(S_{01} + S_{10}) - 2k_{\text{on}}\langle n \rangle_{00}, \\
 \frac{dS_{01}}{dt} &= (\gamma + k_{\text{off}})(S_{11} - S_{01}) + k_{\text{on}} \left[ \langle n \rangle_{00} - \langle n \rangle_{01} \right], \\
 \frac{dS_{10}}{dt} &= (\gamma + k_{\text{off}})(S_{11} - S_{10}) + k_{\text{on}} \left[ \langle n \rangle_{00} - \langle n \rangle_{10} \right], \\
 \frac{dS_{11}}{dt} &= -2(\gamma + k_{\text{off}})S_{11} + k_{\text{on}} \left[ \langle n \rangle_{01} + \langle n \rangle_{10} \right].
 \end{aligned} \tag{A9-2}$$

1110 Multiplying both sides of Eqn. A9-1 by  $n$  and summing over all values of  $(m, n)$  we get the  
 1111 time evolution of free TF protein in each state ( $\langle n \rangle_{ij} = \sum_{m,n} n P_{i,j}(n, m, t)$ )

$$\begin{aligned}
 \frac{d\langle n \rangle_{00}}{dt} &= \alpha S_{00} - \gamma \langle n \rangle_{00} + \gamma [\langle n \rangle_{01} + \langle n \rangle_{10}] + k_{\text{off}} [\langle n+1 \rangle_{01} + \langle n+1 \rangle_{10}] - 2k_{\text{on}} \langle n^2 \rangle_{00} \\
 \frac{d\langle n \rangle_{01}}{dt} &= \alpha S_{01} - \gamma \langle n \rangle_{01} + \gamma [\langle n \rangle_{11} - \langle n \rangle_{01}] + k_{\text{off}} [\langle n+1 \rangle_{11} - \langle n \rangle_{01}] + k_{\text{on}} [\langle n(n-1) \rangle_{00} - \langle n^2 \rangle_{01}] \\
 \frac{d\langle n \rangle_{10}}{dt} &= -\gamma \langle n \rangle_{10} + \gamma [\langle n \rangle_{11} - \langle n \rangle_{10}] + k_{\text{off}} [\langle n+1 \rangle_{11} - \langle n \rangle_{10}] + k_{\text{on}} [\langle n(n-1) \rangle_{00} - \langle n^2 \rangle_{10}] \\
 \frac{d\langle n \rangle_{11}}{dt} &= -\gamma \langle n \rangle_{11} - 2\gamma \langle n \rangle_{11} - 2k_{\text{off}} \langle n \rangle_{11} + k_{\text{on}} [\langle n(n-1) \rangle_{01} + \langle n(n-1) \rangle_{10}].
 \end{aligned}
 \tag{A9-3}$$

1116 Similarly, multiplying both sides of Eqn. A9-1 by  $m$  and summing over all values of  $(m, n)$   
 1117 we obtain the time evolution of target protein in each state ( $\langle m \rangle_{ij} = \sum_{m,n} m P_{i,j}(n, m, t)$ )

$$\begin{aligned}
 \frac{d\langle m \rangle_{00}}{dt} &= \alpha S_{00} - \gamma \langle m \rangle_{00} + \gamma [\langle m \rangle_{01} + \langle m \rangle_{10}] + k_{\text{off}} [\langle m \rangle_{01} + \langle m \rangle_{10}] - 2k_{\text{on}} \langle mn \rangle_{00} \\
 \frac{d\langle m \rangle_{01}}{dt} &= -\gamma \langle m \rangle_{01} + \gamma [\langle m \rangle_{11} - \langle m \rangle_{01}] + k_{\text{off}} [\langle m \rangle_{11} - \langle m \rangle_{01}] + k_{\text{on}} [\langle mn \rangle_{00} - \langle mn \rangle_{01}] \\
 \frac{d\langle m \rangle_{10}}{dt} &= \alpha S_{10} - \gamma \langle m \rangle_{01} + \gamma [\langle m \rangle_{11} - \langle m \rangle_{10}] + k_{\text{off}} [\langle m \rangle_{11} - \langle m \rangle_{10}] + k_{\text{on}} [\langle mn \rangle_{00} - \langle mn \rangle_{01}] \\
 \frac{d\langle m \rangle_{11}}{dt} &= -\gamma \langle m \rangle_{11} - 2\gamma \langle m \rangle_{11} - 2k_{\text{off}} \langle m \rangle_{11} + k_{\text{on}} [\langle mn \rangle_{01} + \langle mn \rangle_{10}].
 \end{aligned}
 \tag{A9-4}$$

1122 The rate equation for total number of TF (sum of the free TFs in each state and the bound  
 1123 TFs in state 2, 3, and 4) and the total target protein can be written as

$$\begin{aligned}
 \frac{d\langle n \rangle}{dt} &= \frac{d}{dt} [\langle n \rangle_{00} + \langle n \rangle_{01} + \langle n \rangle_{10} + \langle n \rangle_{11} + S_{01} + S_{10} + 2S_{11}] \\
 &= \alpha(S_{00} + S_{01}) - \gamma \langle n \rangle \\
 \frac{d\langle m \rangle}{dt} &= \frac{d}{dt} [\langle m \rangle_{00} + \langle m \rangle_{01} + \langle m \rangle_{10} + \langle m \rangle_{11}] \\
 &= \alpha(S_{00} + S_{10}) - \gamma \langle m \rangle.
 \end{aligned}
 \tag{A9-5}$$

1128 The steady state expression for total TF and target can be obtained by setting Eqn. A9-5  
 1129 to zero which yields

$$\begin{aligned}
 \langle n \rangle_{\text{ss}} &= \frac{\alpha}{\gamma} (S_{00} + S_{01}) = C_0 (S_{00} + S_{01}), \\
 \langle m \rangle_{\text{ss}} &= \frac{\alpha}{\gamma} (S_{00} + S_{10}) = C_0 (S_{00} + S_{10}),
 \end{aligned}
 \tag{A9-6}$$

1134 where  $C_0 = \alpha/\gamma$  is the constitutive protein expression. The asymmetry defined as the  
 1135 difference of fold change in expression of target and TF gene expression is given by

$$\begin{aligned}
 \text{Asymmetry} &= \text{FC}_{\text{Target}} - \text{FC}_{\text{TF}}, \\
 &= \frac{\langle m \rangle_{\text{ss}}}{C_0} - \frac{\langle n \rangle_{\text{ss}}}{C_0}, \\
 &= S_{10} - S_{01}.
 \end{aligned}
 \tag{A9-7}$$

1140 The asymmetry in TF and target regulation simply depends on the difference of occupancy  
 1141 in the states where TF gene is bound and where the target gene is bound. Furthermore, the  
 1142 steady state occupancies are given by (setting Eqns. A9-2 to zero)

$$\begin{aligned}
 1143 \quad S_{01} &= S_{11} + \frac{k_{\text{on}}}{(\gamma + k_{\text{off}})} \left[ \langle n \rangle_{00} - \langle n \rangle_{01} \right], \\
 1144 \quad S_{10} &= S_{11} + \frac{k_{\text{on}}}{(\gamma + k_{\text{off}})} \left[ \langle n \rangle_{00} - \langle n \rangle_{10} \right], \\
 1145 \quad S_{11} &= \frac{k_{\text{on}}}{2(\gamma + k_{\text{off}})} \left[ \langle n \rangle_{01} + \langle n \rangle_{10} \right].
 \end{aligned}
 \tag{A9-8}$$

1148 The asymmetry using Eqns. A9-7 and A9-8 is then given by  
 1147  
 1149

$$1150 \quad \text{Asymmetry} = \frac{k_{\text{on}}}{(\gamma + k_{\text{off}})} \left[ \langle n \rangle_{01} - \langle n \rangle_{10} \right].
 \tag{A9-9}$$

1152 Eqn. A9-9 clearly demonstrates that the asymmetry in TF and target expression arises  
 1153 from the difference in the free TF concentration in state 2 (only target gene bound) and  
 1154 state 3 (only TF gene bound). Analytical expression for free TFs in different state cannot be  
 1155 determined explicitly as it can be seen from the Eqns. A9-3 and A9-4 that the mean protein  
 1156 ( $\langle n \rangle$ ,  $\langle m \rangle$ ) depends on the higher order moments ( $\langle n^2 \rangle$ ,  $\langle mn \rangle$ ) which then depends on the next  
 1157 higher order moments and so on.

1158 **Appendix 10**1159 **Modified ODEs for the minimal model**

1160 The asymmetry, as explained in the main text and evident from Eqn. A9-9, appears due  
 1161 to the difference in the TF concentration when only the TF gene is occupied and when  
 1162 only the target gene is occupied. The general deterministic approach does not capture  
 1163 this asymmetry due to the mean field assumption of uniform TF concentration in all the  
 1164 states. To incorporate the difference in TF concentration in the deterministic model we now  
 1165 specifically assume the four state model; 1) both the TF gene and target gene are free to  
 1166 express, 2) TF gene is bound by TF, 3) target gene is bound by TF, and 4) both the genes are  
 1167 bound by TF. The number of cells in each state are  $S_1, S_2, S_3$ , and  $S_4$  and the total population  
 1168 ( $S$ ) is constant. The free TF and total target protein number in each states are  $(n_1, m_1)$ ,  
 1169  $(n_2, m_2)$ ,  $(n_3, m_3)$ , and  $(n_4, m_4)$  such that the average free TFs in each cell is  $\langle n \rangle_i = n_i/S_i$  and average  
 1170 target protein in each cell is  $\langle m \rangle_i = m_i/S_i$ . State 1 switches to state 2 and 3 when a free TF  
 1171 binds to the free promoter of TF gene or target gene. State 2 and state 3 switch to state 1  
 1172 when a bound TF unbinds or degrade from the gene. State 2 and state 3 also switch to state  
 1173 4 due to TF binding. Finally, state 4 switches to state 2 and state 3 when a bound TF unbinds  
 1174 or degrade from the gene.

1175 Change in cell number due to the reactions that switch the cells from state  $i$  to state  $j$   
 1176 causing an increase(state  $j$ ) or decrease (state  $i$ ) in the cell population per unit time are

$$1177 \text{ Binding : } k_{\text{on}} \langle n_i \rangle S_i = k_{\text{on}} \frac{n_i}{S_i} S_i = k_{\text{on}} n_i$$

$$1178 \text{ Unbinding : } k_{\text{off}} S_i \tag{A10-1}$$

$$1179 \text{ Degradation of TF from gene : } \gamma S_i$$

1180  
 1181 When a TF binds to a promoter of TF gene or target gene in state  $i$  switching the cells  
 1182 to state  $j$  the number of free TF of the cells in state  $j$  increases by the  $(\langle n \rangle_j - 1)$  times the  
 1183 number of cell switched ( $k_{\text{on}} n_i$ ) and the number of target protein increases by  $\langle m \rangle_j k_{\text{on}} n_i$ . It  
 1184 is to be noted that a binding event decreases the average free TF pool by one in the cells  
 1185 which switch from state  $i$  to state  $j$ . In the process the cells in state  $i$  loses  $\langle n \rangle_i k_{\text{on}} n_i$  number  
 1186 of free TFs and  $\langle m \rangle_i k_{\text{on}} n_i$  number of target. Similarly, when a TF unbinds from a promoter  
 1187 switching state  $i$  to state  $j$  the number of free TFs of cells in state  $j$  increases by  $(\langle n \rangle_j + 1)$   
 1188 times the number of cell switched ( $k_{\text{off}} S_i$ ) and the number of free TFs of each cell in state  $i$   
 1189 goes down by  $\langle n \rangle_i$  times the number of cell switched. The target protein number of cells in  
 1190 state  $i$  goes down by  $\langle m \rangle_i k_{\text{off}} n_i$  and increase by the same amount in state  $j$ . Degradation of  
 1191 bound TF changes the free TF number by  $\langle n \rangle_i \gamma S_i$  and target protein number by  $\langle m \rangle_i \gamma S_i$ . The  
 1192 change in protein number for all the reactions are listed in **Appendix 10 Table 1**.

1193 The set of ODEs describing the time evolution of the cell populations ( $S_i$ ) in each state is  
 1194 then given by

$$1195 \frac{dS_1}{dt} = -2k_{\text{on}} n_1 + (k_{\text{off}} + \gamma)(S_2 + S_3),$$

$$1196 \frac{dS_2}{dt} = k_{\text{on}} n_1 - k_{\text{on}} n_2 + (k_{\text{off}} + \gamma)(S_4 - S_2),$$

$$1197 \frac{dS_3}{dt} = k_{\text{on}} n_1 - k_{\text{on}} n_3 + (k_{\text{off}} + \gamma)(S_4 - S_3),$$

$$1198 \frac{dS_4}{dt} = k_{\text{on}} n_2 + k_{\text{on}} n_3 - 2(k_{\text{off}} + \gamma)S_4. \tag{A10-2}$$

1199

The rate equations for free TF number can be written as

$$\begin{aligned}
 \frac{dn_1}{dt} &= \alpha S_1 - \gamma n_1 + k_{\text{off}}(n_2 + S_2) + k_{\text{off}}(n_3 + S_3) - 2k_{\text{on}} \frac{n_1^2}{S_1} + \gamma(n_2 + n_3), \\
 \frac{dn_2}{dt} &= \alpha S_2 - \gamma n_2 + k_{\text{off}}(n_4 + S_4) - k_{\text{off}}n_2 + k_{\text{on}} \frac{n_1(n_1 - S_1)}{S_1} - k_{\text{on}} \frac{n_2^2}{S_2} + \gamma(n_4 - n_2), \\
 \frac{dn_3}{dt} &= -\gamma n_3 + k_{\text{off}}(n_4 + S_4) - k_{\text{off}}n_3 + k_{\text{on}} \frac{n_1(n_1 - S_1)}{S_1} - k_{\text{on}} \frac{n_3^2}{S_3} + \gamma(n_4 - n_3), \\
 \frac{dn_4}{dt} &= -\gamma n_4 - 2k_{\text{off}}n_4 + k_{\text{on}} \frac{n_2(n_2 - S_2)}{S_2} + k_{\text{on}} \frac{n_3(n_3 - S_3)}{S_3} - 2\gamma n_4,
 \end{aligned} \tag{A10-3}$$

1204

and the rate equations for target protein number is given by

$$\begin{aligned}
 \frac{dm_1}{dt} &= \alpha S_1 - \gamma m_1 + k_{\text{off}}m_2 + k_{\text{off}}m_3 - 2k_{\text{on}} \frac{m_1 n_1}{S_1} + \gamma(m_2 + m_3), \\
 \frac{dm_2}{dt} &= -\gamma m_2 + k_{\text{off}}m_4 - k_{\text{off}}m_2 + k_{\text{on}} \frac{m_1 n_1}{S_1} - k_{\text{on}} \frac{m_2 n_2}{S_2} + \gamma(m_4 - m_2), \\
 \frac{dm_3}{dt} &= \alpha S_3 - \gamma m_3 + k_{\text{off}}m_4 - k_{\text{off}}m_3 + k_{\text{on}} \frac{m_1 n_1}{S_1} - k_{\text{on}} \frac{m_3 n_3}{S_3} + \gamma(m_4 - m_3), \\
 \frac{dm_4}{dt} &= -\gamma m_4 - 2k_{\text{off}}m_4 + k_{\text{on}} \frac{m_2 n_2}{S_2} + k_{\text{on}} \frac{m_3 n_3}{S_3} - 2\gamma m_4.
 \end{aligned} \tag{A10-4}$$

1209

Using Eqns. A10-2-A10-4, the rate equations for total TF and target protein can be written

1210

as

$$\begin{aligned}
 \frac{dn}{dt} &= \frac{d}{dt}(n_1 + n_2 + n_3 + n_4 + S_2 + S_3 + 2S_4), \\
 &= \alpha(S_1 + S_2) - \gamma n, \\
 \frac{dm}{dt} &= \frac{d}{dt}(m_1 + m_2 + m_3 + m_4), \\
 &= \alpha(S_1 + S_3) - \gamma m.
 \end{aligned} \tag{A10-5}$$

1215

The steady state concentration for total TF and target protein is obtained by setting Eqn. A10-5 to zero which gives

1216

1217

1218

1219

1220

$$\begin{aligned}
 n_{\text{ss}} &= \frac{\alpha}{\gamma}(S_{1,\text{ss}} + S_{2,\text{ss}}) = C_0(S_{1,\text{ss}} + S_{2,\text{ss}}), \\
 m_{\text{ss}} &= \frac{\alpha}{\gamma}(S_{1,\text{ss}} + S_{3,\text{ss}}) = C_0(S_{1,\text{ss}} + S_{3,\text{ss}}).
 \end{aligned} \tag{A10-6}$$

1221

Here,  $C_0 = \alpha/\gamma$  is the protein number of unregulated gene (constitutive expression). The steady state number of cells in states in terms of free TF number can be obtained by setting Eqn. A10-2 to zero and is given by

1222

1223

1224

1225

1226

1227

$$\begin{aligned}
 S_{1,\text{ss}} &= S - (S_{2,\text{ss}} + S_{3,\text{ss}} + S_{4,\text{ss}}) = S - \frac{k_{\text{on}}}{2(k_{\text{off}} + \gamma)}(4n_{1,\text{ss}} + n_{2,\text{ss}} + n_{3,\text{ss}}), \\
 S_{2,\text{ss}} &= \frac{k_{\text{on}}}{2(k_{\text{off}} + \gamma)}(2n_{1,\text{ss}} - n_{2,\text{ss}} + n_{3,\text{ss}}) \\
 S_{3,\text{ss}} &= \frac{k_{\text{on}}}{2(k_{\text{off}} + \gamma)}(2n_{1,\text{ss}} + n_{2,\text{ss}} - n_{3,\text{ss}}) \\
 S_{4,\text{ss}} &= \frac{k_{\text{on}}}{2(k_{\text{off}} + \gamma)}(n_{2,\text{ss}} + n_{3,\text{ss}}).
 \end{aligned} \tag{A10-7}$$

1228  
1229  
1230  
1231

Setting  $S = 1$  converts the number of cells ( $S_i$ ) to occupancy of the cell in each state and  $n_i, m_i$  to fractional average of free TF and target protein per cell, i.e.  $n_i = n_{ss} S_i$  and  $m_i = m_{ss} S_i$ . The asymmetry defined as the difference of fold change in expression of target and TF gene expression is given by

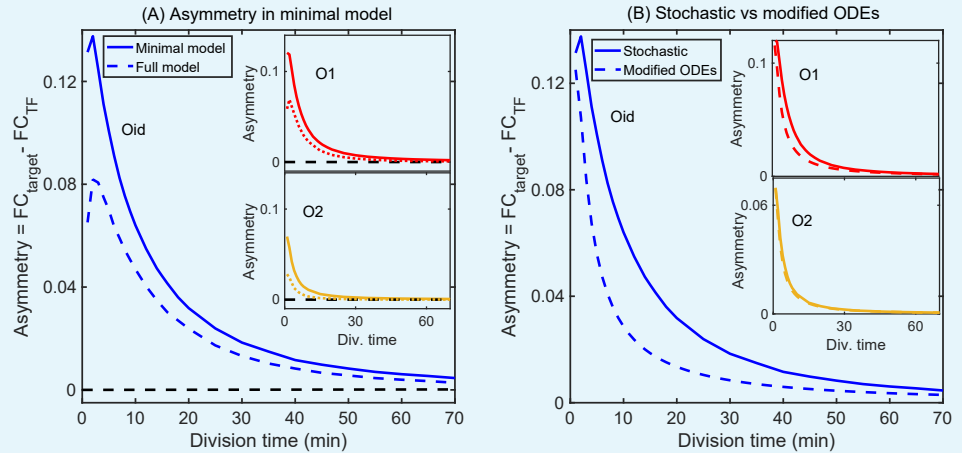
1232  
1233  
1234  
1235

$$\begin{aligned} \text{Asymmetry} &= FC_{\text{Target}} - FC_{\text{TF}}, \\ &= \frac{m_{ss}}{C_0} - \frac{n_{ss}}{C_0}, \\ &= S_{3,ss} - S_{2,ss}, \\ &= \frac{k_{\text{on}}}{k_{\text{off}} + \gamma} (n_{2,ss} - n_{3,ss}). \end{aligned} \tag{A10-8}$$

1236  
1237  
1238  
1239  
1240  
1241  
1242

It is important to note that the same set of ODEs (Eqns. A10-2-A10-4) can be derived from CME by setting the variance and covariance of protein number in each state to zero. This modified ODEs predicts asymmetry between the TF and target expressions as shown in **Appendix 10 Figure 1A**, however, the predicted asymmetry doesn't match quantitatively with the CME predictions (see **Appendix 10 Figure 1B**). This discrepancy arises because of the fluctuations in the protein number in each state which is not considered in the modified ODEs.

1243  
1244  
1245  
1246  
1247  
1248  
1249  
1250  
1251  
1252  
1253  
1254  
1255



**Appendix 10 Figure 1. Minimal model of autoregulation.** (A) Asymmetry predicted from a minimal model without intermediate transcription steps and decoy binding sites using stochastic simulations (solid lines in blue, red and yellow for Oid, O1 and O2 binding sites, respectively). The asymmetry follows similar trend as predicted in the complete stochastic model (shown as dashed lines). Stronger binding site (Oid, shown in solid blue line) shows higher asymmetry than a weak binding site (O2, shown in solid yellow line). Also, asymmetry decreases as the growth rate is increased. Black dashed line corresponds to the deterministic counterpart of the stochastic reaction systems. Again, we do not find any asymmetry in TF and target regulation from the deterministic solution. (B) Modified ODEs with the inclusion of four states each having a different TF concentration predict asymmetry (dashed lines for different binding sites Oid (blue), O1 (red), and O2 (yellow)). However, the quantitative values disagree from the stochastic simulations of minimal model shown as solid lines.

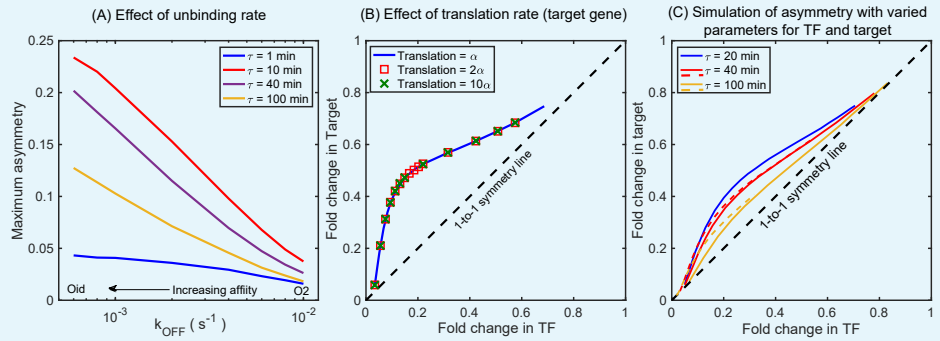
1256  
1257

Reaction	Increase in free TF	Decrease in free TF
Production in active state	$\alpha S_i$	-
Degradation of free TF	-	$\gamma n_i$
Binding	$\left(\frac{n_i}{S_i} - 1\right) k_{\text{on}} n_i = k_{\text{on}} \frac{n_i(n_i - S_i)}{S_i}$	$\frac{n_i}{S_i} k_{\text{on}} n_i = k_{\text{on}} \frac{n_i^2}{S_i}$
Unbinding	$\left(\frac{n_i}{S_i} + 1\right) k_{\text{off}} S_i = k_{\text{off}}(n_i + S_i)$	$\left(\frac{n_i}{S_i} + 1\right) k_{\text{off}} S_i = k_{\text{off}}(n_i + S_i)$
Degradation of TF from gene	$\frac{n_i}{S_i} \gamma S_i = \gamma n_i$	$\frac{n_i}{S_i} \gamma S_i = \gamma n_i$
	Increase in target	Decrease in target
Production in active state	$\alpha S_i$	-
Degradation of target	-	$\gamma m_i$
Binding	$\frac{m_i}{S_i} k_{\text{on}} n_i = k_{\text{on}} \frac{m_i n_i}{S_i}$	$\frac{m_i}{S_i} k_{\text{on}} n_i = k_{\text{on}} \frac{m_i n_i}{S_i}$
Unbinding	$\frac{m_i}{S_i} k_{\text{off}} S_i = k_{\text{off}} m_i$	$\frac{m_i}{S_i} k_{\text{off}} S_i = k_{\text{off}} m_i$
Degradation of TF from gene	$\frac{m_i}{S_i} \gamma S_i = \gamma m_i$	$\frac{m_i}{S_i} \gamma S_i = \gamma m_i$

1258  
1260

**Appendix 10 Table 1.** Change in free TF and target protein number for the reactions describing the minimal model

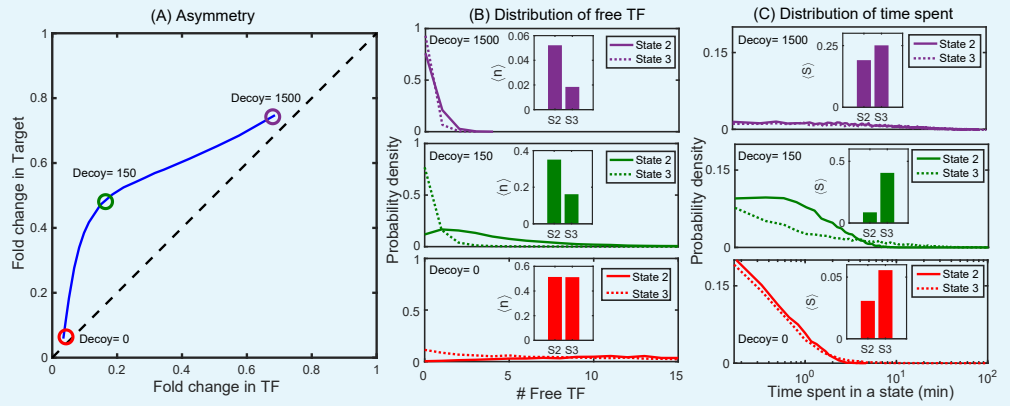
1261 **Appendix 11**



1262  
1263  
1264  
1265  
1266  
1267  
1268  
1269  
1270  
1271  
1272  
1273  
1274  
1276

**Appendix 11 Figure 1. Simulations showing the effects of rate parameters on asymmetry. (A)** Effect of TF unbinding rate ( $k_{OFF}$ ) on asymmetry. Irrespective of the  $k_{OFF}$ , the maximum asymmetry decreases monotonically. **(B)** Asymmetry is not affected by difference in translation rate between the TF gene and the target gene. Blue solid curve represents asymmetry obtained from simulations where the translation rate of TF gene and the target gene is exactly same. The data points are generated with a translation rate of target gene twice (red square) and ten times (green cross) that of the TF gene and fall exactly on the blue curve showing no deviation. **(C)** Asymmetry for different growth rate ( $\tau$ ) with varying transcription rate, translation rate, and mRNA stability. Stochastic simulation performed using the kinetic parameters listed in *Bremer and Dennis (2008)* for  $\tau$  being 20 (blue line), 40 (red line), and 100 (yellow line) minutes. Dashed lines show the asymmetry for  $\tau$  = 40 min and 100 min for the rate parameters same as  $\tau$  = 20 min. The qualitative ordering and features of the asymmetry curve is not impacted by the changes in the kinetic parameters such as transcription rate, translation rate, and mRNA stability due to change in growth rates.

1277 **Appendix 12**



1278  
1279  
1280  
1281  
1282  
1283  
1284  
1285  
1286  
1288

**Appendix 12 Figure 1. Distributions of free TFs and time spent in different promoter states. (A)** Typical asymmetry plot obtained from simulations for Oid binding site with division time  $\tau = 25$  min. **(B-C)** Distribution of free TFs and time spent in state 2 (S2) and state 3 (S3) for varying level of asymmetry corresponding to different decoy number as shown in panel (A). The plots in red, green and purple correspond to no decoys (low asymmetry), 150 decoy (maximum asymmetry) and 1500 decoy (low asymmetry). Insets in (B) are steady state fractional average of free TFs in state 2 and state 3 obtained from stochastic simulations using equation  $\langle n \rangle = \sum_{m,n} n P_{i,j}$ , where  $P_{i,j}$  is the probability of having  $m$  target protein and  $n$  free TF in the promoter state  $(i,j)$ ; see Appendix 9. Insets in (C) are TF-occupancy in state 2 and state 3 defined as  $\langle \phi \rangle = \sum_{m,n} P_{i,j}$ .